

Possible Liquid-Nitrogen-Temperature Superconductivity Driven by Perpendicular Electric Field in the Single-Bilayer Film of $\text{La}_3\text{Ni}_2\text{O}_7$ at Ambient Pressure

Zhi-Yan Shao,^{1,*} Jia-Heng Ji,^{1,*} Congjun Wu,^{2,3,4,5} Dao-Xin Yao,⁶ and Fan Yang^{1,†}

¹*School of Physics, Beijing Institute of Technology, Beijing 100081, China*

²*New Cornerstone Science Laboratory, Department of Physics,*

School of Science, Westlake University, Hangzhou 310024, Zhejiang, China

³*Institute for Theoretical Sciences, Westlake University, Hangzhou 310024, Zhejiang, China*

⁴*Key Laboratory for Quantum Materials of Zhejiang Province,*

School of Science, Westlake University, Hangzhou 310024, Zhejiang, China

⁵*Institute of Natural Sciences, Westlake Institute for Advanced Study, Hangzhou 310024, Zhejiang, China*

⁶*Guangdong Provincial Key Laboratory of Magnetoelectric Physics and Devices,*

State Key Laboratory of Optoelectronic Materials and Technologies,

Center for Neutron Science and Technology, School of Physics,

Sun Yat-Sen University, Guangzhou, 510275, China

Abstract: Recently, high-temperature superconductivity (HTSC) is found in the $\text{La}_3\text{Ni}_2\text{O}_7/\text{SrLaAlO}_4$ ultrathin film with critical temperature T_c above the McMillan limit at ambient pressure (AP). It is eager to enhance T_c of $\text{La}_3\text{Ni}_2\text{O}_7$ at AP. We propose that a perpendicular electric field strongly enhances T_c in the single-bilayer film of $\text{La}_3\text{Ni}_2\text{O}_7$ at AP. Under electric field, the layer with lower potential energy will accept electrons flowing from the other layer to fill in the $\text{Ni-}3d_{x^2-y^2}$ orbitals, as the nearly half-filled $\text{Ni-}3d_{z^2}$ orbital cannot accommodate more electrons. With the enhancement of the filling fraction in the $3d_{x^2-y^2}$ orbitals in this layer, the interlayer s -wave pairing is suppressed, but the intralayer d -wave pairing in this layer is strongly enhanced. We numerically verify this idea and yield that an imposed voltage of about $0.1 \sim 0.2$ volt between layers is enough to realize liquid-nitrogen-temperature HTSC in this single bilayer at AP. Our results appeal for experimental verification.

INTRODUCTION

The discovery of superconductivity (SC) with critical temperature T_c above the boiling point of liquid nitrogen (≈ 77 K) in the pressurized $\text{La}_3\text{Ni}_2\text{O}_7$ [1–9] has attracted great interests [10–144]. This discovery has sparked the exploration of high-temperature SC (HTSC) in Ruddlesden-Popper phase multilayer nickelates, resulting in the discovery of SC in the pressurized $\text{La}_4\text{Ni}_3\text{O}_{10}$ [39–45], which together with the previously synthesized infinite-layer nickelates $\text{Nd}_{1-x}\text{Sr}_x\text{NiO}_2$ [46–49] have established a new family of SC other than cuprates and iron-based superconductors. However, the high pressure (HP) circumstance not only strongly hinders the experimental detection of the samples but also brings difficulties in the application of SC in industry. Very recently, the $\text{La}_3\text{Ni}_2\text{O}_7$ ultrathin film with a few layers of unit cell grown on the SrLaAlO_4 (SLAO) substrate has been grown by two different groups independently and SC with T_c above the McMillan limit (≈ 40 K) has been detected at ambient pressure (AP) [132–134], allowing various experimental investigation of the pairing mechanism in this material, attracting a lot of interests [135–144]. It is now eager to enhance the T_c of this material at AP. Here we propose a viable approach to realize T_c above the boiling point of liquid nitrogen in the $\text{La}_3\text{Ni}_2\text{O}_7$ single-bilayer film at AP.

Presently, the pairing mechanism in the $\text{La}_3\text{Ni}_2\text{O}_7$, either in the bulk material under HP [74–100, 104–108, 125–128] or in the ultrathin film at AP [135, 138,

140, 143], is still under debate. Density-functional-theory (DFT) based first-principle calculations have suggested that the low-energy orbitals are mainly $\text{Ni-}3d_{z^2}$ and $3d_{x^2-y^2}$, which are nearly half- and quarter-filled [50–58, 61]. Various experiments have revealed the strongly-correlated characteristic of the material [14, 16, 22, 24, 25, 28, 31, 32]. Particularly, the optical study reveals significant reduction of the electron kinetic energy which places the system in the proximity of the Mott phase [25]; the angle-resolved photoemission spectroscopy uncovers strong band renormalization caused by electron correlation [28]; the linearly temperature-dependent resistivity suggests “strange-metal” behavior [2]. Therefore, we take a strong-coupling view of the system. Under the strong Hubbard repulsion, the nearly half-filled $3d_{z^2}$ electrons can almost be viewed as localized spins. Therefore, the main carrier of SC should be the $3d_{x^2-y^2}$ electrons, which subject to the in-plane superexchange interaction just mimic the 50% hole-doped cuprates. However, it is a problem how HTSC can emerge under such a high doping level. The key physics lies in the important role played by the $3d_{z^2}$ orbitals. Through strong interlayer perpendicular superexchange, the $3d_{z^2}$ electrons form interlayer pairing. The interlayer perpendicular superexchange or the interlayer pairing of the $3d_{z^2}$ electrons can be transmitted to the $3d_{x^2-y^2}$ electrons through the Hund’s rule [79, 80, 82, 87, 92, 93, 95–98, 100, 107, 108] or the nearest-neighbor (NN) hybridization [65, 83, 86, 87, 91, 98, 105, 107, 108] or both. Under such view, the role of pressure in enhancing the T_c lies

in the enhancement of the interlayer perpendicular superexchange, the inter-orbital hybridization, or both.

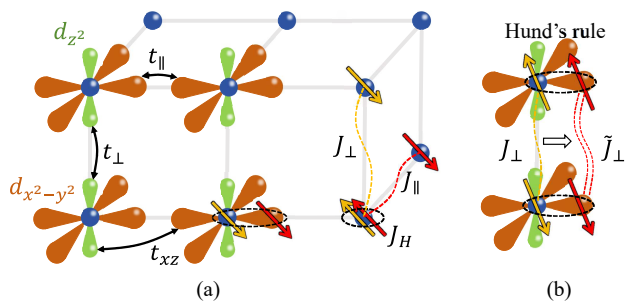


FIG. 1. Schematic diagrams of the model. (a) Schematic diagram for the dominant hopping integrals and superexchange interactions between the E_g orbitals in $\text{La}_3\text{Ni}_2\text{O}_7$. (b) Schematic diagram illustrating that the Hund's rule coupling transmits the interlayer perpendicular superexchange interaction J_\perp between the $3d_{z^2}$ orbitals to the effective one \tilde{J}_\perp between the $3d_{x^2-y^2}$ orbitals.

In this work, we propose an alternative approach to realize HTSC with T_c above the boiling point of liquid nitrogen in the ultrathin film of $\text{La}_3\text{Ni}_2\text{O}_7$ at AP. Here we consider the thinnest limit, i.e. a single bilayer film of $\text{La}_3\text{Ni}_2\text{O}_7$, and realize the goal by introducing charge transfer with a perpendicular electric field, which let the electrons flow from the high-energy layer to the low-energy layer, similar to the mechanism for the spontaneous charge transfer in oxide heterostructures [145–150]. The external electric field based approach avoids introducing disorder as in chemical doping [151] or exhibiting orbital selectivity based on symmetry [152], demonstrating exceptional performance in the field of twisted multilayer graphene materials [153–155]. We can impose a perpendicular electric field, say pointing upward, in this single bilayer, so that electrons from the top layer will flow to the bottom layer. These electrons will fill the $3d_{x^2-y^2}$ orbitals in the bottom layer as the nearly half-filled $3d_{z^2}$ orbitals there cannot accommodate more electrons. The enhancement of the bottom-layer $3d_{x^2-y^2}$ electron number will first suppress the interlayer s -wave SC due to mismatch of the electron numbers between the two layers, similar with the case in which an imposed Zeeman field acting on the spin leads to mismatch of the electron numbers between the two spin species and thus suppresses singlet pairing, and then promptly lead to the intra-bottom-layer d -wave SC with strongly enhanced T_c . To test this idea, we have performed a combined simplified single orbital study and a comprehensive two orbital study, which consistently yield that a voltage of experimentally achievable levels (around 0.1 ~ 0.2 volt predicted by the mean-field calculations) between the two layers is enough to induce d -wave SC with T_c above the boiling point of liquid nitrogen in the bottom layer. Intriguingly, the d -wave SC carried by the bot-

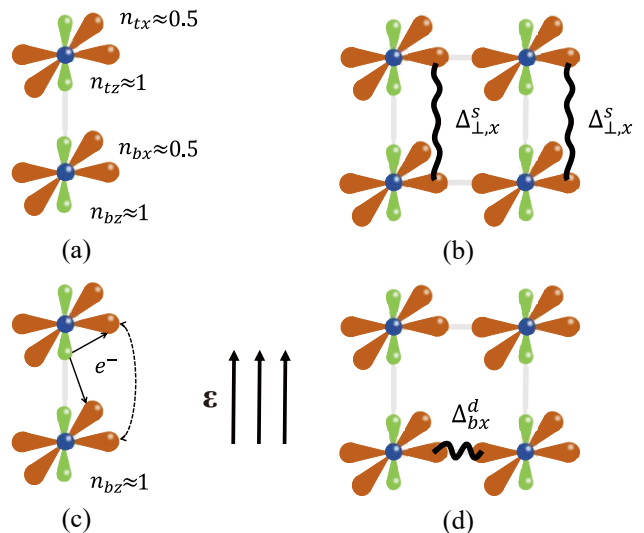


FIG. 2. Schematic diagrams of particle number and pairing configuration before and after introducing perpendicular electric field. (a) Particle numbers of the four E_g orbitals within an unit cell without electric field. (b) The dominant pairing configuration for (a). (c) Schematic diagram showing how the electrons flow under the perpendicular electric field ϵ pointing upward. (d) The dominant pairing configuration for (c).

tom layer $3d_{x^2-y^2}$ electrons coexists with the interlayer s -wave pseudo gap carried by the $3d_{z^2}$ electrons in the mixing ratio of 1 : i , breaking time-reversal symmetry. Our proposal potentially provides a viable approach to realize HTSC with T_c above the boiling point of liquid nitrogen in the single bilayer film of $\text{La}_3\text{Ni}_2\text{O}_7$.

RESULTS

Consideration and a Simplified Study

The $\text{La}_3\text{Ni}_2\text{O}_7$ ultrathin film grown on the SLAO substrate form a bilayer square lattice [135, 137]. As illustrated in Fig. 1 (a), the leading hopping integrals are the interlayer hopping of the $3d_{z^2}$ electrons t_\perp and the intralayer NN hopping of the $3d_{x^2-y^2}$ electrons t_\parallel . Under strong Hubbard U , these hopping terms can induce the effective superexchange J_\perp and J_\parallel through $J \approx \frac{4t^2}{U}$. Under the Hund's rule coupling J_H , the spins of the two orbitals are inclined to be parallel aligned, as illustrated in Fig. 1 (b), which partly transmits the interlayer perpendicular superexchange J_\perp between the $3d_{z^2}$ orbitals to the $3d_{x^2-y^2}$ orbitals as $\tilde{J}_\perp = \alpha J_\perp$ with $\alpha \in (0, 1)$ describing the efficiency of this process and related to the strength of Hund's coupling J_H . In addition, there exists intralayer NN- hybridization t_{xz} between the two orbitals. As shown in Fig. 2 (a, b), the nearly quarter-filled $3d_{x^2-y^2}$ electrons subject to J_\parallel and \tilde{J}_\perp form interlayer-dominant pairing [79].

Now let us turn on the upward electric field ϵ , forcing electrons downward, as shown in Fig. 2 (c, d). In the top layer, since the $3d_{z^2}$ orbitals host larger density of state (DOS) than the $3d_{x^2-y^2}$ orbitals, they will donate more electrons. Most of these donated electrons will fill the $3d_{x^2-y^2}$ orbitals in the bottom layer, as the nearly half-filled $3d_{z^2}$ orbitals there cannot accommodate more electrons. A minority of the donated electrons can also be accepted by the top-layer $3d_{x^2-y^2}$ orbitals.

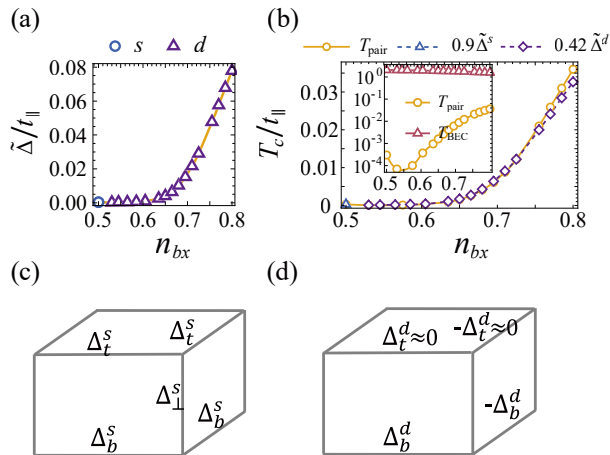


FIG. 3. The SBMF results for the single-orbital model. (a) The pairing amplitude $\tilde{\Delta}$ (in unit of $t_{||}$) as function of the bottom-layer particle number per site n_{bx} . Different pairing symmetries are distinguished by color. (b) The T_c as function of n_{bx} , in comparison with $0.42\tilde{\Delta}$ for the d -wave and $0.9\tilde{\Delta}$ for the s -wave regime. Inset: the spinon pairing temperature T_{pair} and the holon condensation temperature T_{BEC} as function of n_{bx} . In (a,b), we set $J_{||} = 0.4t_{||}$ and $\tilde{J}_{\perp} = (1 - \delta_{tz}) \times 1.3J_{||}$. (c)-(d) The pairing configurations of the s -wave and d -wave, respectively.

Even with doped holes under ϵ , the top-layer $3d_{z^2}$ electrons cannot carry SC: Firstly, lacking pairing interaction, they cannot form intralayer pairing. Secondly, although they can pair with the localized bottom-layer $3d_{z^2}$ electrons, such pairs cannot coherently move, only resulting in the pseudo-gap. Therefore, the SC under ϵ can only be carried by the $3d_{x^2-y^2}$ orbitals. As the filling fractions of the $3d_{x^2-y^2}$ orbitals in the two layers are different, their Fermi levels are relatively shift, leading to mismatch of their Fermi surfaces (FSSs), which will suppress their interlayer pairing. Here the perpendicular electric field acts as a “pseudo-Zeeman field” acting on the layer index, just like the Zeeman field acting on the spin degree of freedom. The bottom-layer $3d_{x^2-y^2}$ orbitals will form d -wave SC, mimicking the cuprates, as shown in Fig. 2 (d). When ϵ is strong enough so that the filling fraction of the bottom-layer $3d_{x^2-y^2}$ orbitals is near that of the optimal doped cuprates, d -wave HTSC with strongly enhanced T_c will be achieved in this layer, and the top layer will also acquire SC below T_c through

proximity.

Based on the above general consideration, we first conduct the following simplified model study including only the $3d_{x^2-y^2}$ -orbital, with the $3d_{z^2}$ orbital only viewed as a source which tunes the total electron number. The following widely adopted single $3d_{x^2-y^2}$ -orbital bilayer $t - J - J_{\perp}$ model [79, 80, 82, 92, 93, 95, 96, 100] is adopted,

$$H = - t_{||} \sum_{\langle i,j \rangle, \mu, \sigma} \hat{P} \left(c_{i\mu\sigma}^{\dagger} c_{j\mu\sigma} + \text{h.c.} \right) \hat{P} + \sum_{i, \mu} \epsilon_{\mu} n_{i\mu} + J_{||} \sum_{\langle i,j \rangle, \mu} \mathbf{S}_{i\mu} \cdot \mathbf{S}_{j\mu} + \tilde{J}_{\perp} \sum_i \mathbf{S}_{it} \cdot \mathbf{S}_{ib}. \quad (1)$$

Here $c_{i\mu\sigma}^{\dagger}$ creates an electron at site i in the layer μ ($=$ top (t)/bottom (b)) with spin σ , \hat{P} is a projection operator projecting out the double occupancy of all site, and $n_{i\mu}$ or $\mathbf{S}_{i\mu}$ denote the corresponding electron number or spin operator. Only NN- bond $\langle i, j \rangle$ is considered in the summation. The ϵ_{μ} is introduced to control the filling fractions of the two layers under ϵ , with $\epsilon_t - \epsilon_b = \epsilon$. However, as the total particle number of the $d_{x^2-y^2}$ electrons under given ϵ is unknown, we have to assume the ratio $r : 1$ between the electron number flowing from the $3d_{z^2}$ orbitals and that flowing from $3d_{x^2-y^2}$ orbitals in the top layer when solving the model with the standard slave-boson mean-field (SBMF) theory [156], which demonstrates exceptional performance for $\text{La}_3\text{Ni}_2\text{O}_7$ in previous studies [79, 80] that is qualitatively consistent with experimental data [1] and theoretical studies using other numerical methods (like DMRG) [82, 92, 96]. Due to reason of DOS, we assume this ratio to be 2 : 1, with details provided in the Supplementary Information (SI) [157]. Nevertheless, the concrete value of this ratio turns out not to obviously affect the results (see the SI [157]). The filling fractions are fixed under this assumption in the SBMF study. To capture the quantum fluctuation beyond mean-field, the density matrix renormalization group (DMRG) [158, 159] method is also employed, whose results are qualitatively consistent with those of the SBMF study, indicating that the SBMF theory can capture the main features of this system. See details in the **METHODS** and SI [157].

We set $t_{||} = 1$ as the energy unit and $J_{||} = 0.4t_{||}$ in our study. $\tilde{J}_{\perp} = (1 - \delta_{tz}) \times 1.3J_{||}$ is applied in our SBMF study. The results are shown in Fig. 3. Fig. 3 (a) shows the amplitude and symmetry of the ground-state pairing gap as function of the bottom-layer $3d_{x^2-y^2}$ electron number n_{bx} , whose value enhances with ϵ . It is shown that when ϵ or n_{bx} enhances, the pairing amplitude $\tilde{\Delta}$ decays first and then increases. When $n_{bx} = 0.5$, the ground state is confirmed to be interlayer s -wave SC by comparing the energies of states with different symmetries (See SI [157] for more details). Then the s -wave pairing is suppressed by the enhancement of ϵ or n_{bx} because of the mismatch of the FSSs of the two layers

caused by ε , similar to the case of a singlet pairing state placed within a pair-breaking Zeeman field. Therefore, it is also possible that this “pseudo Zeeman field” can drive pair density wave (PDW), just like that the real Zeeman field can drive the Fulde-Ferrell-Larkin-Ovchinnikov state. When $n_{bx} \geq 0.53$, the ground state is an intralayer d -wave SC, with the dominant pairing limited in the bottom layer. It is inspiring that with the enhancement of n_{bx} in this regime, the $\tilde{\Delta}$ enhances promptly, similar to the case in the overdoped cuprates, wherein the enhancement of the filling fraction promptly enhances the pairing strength. The pairing configurations of the two different pairing symmetries are illustrated in Fig. 3 (c-d).

The $T_c \sim n_{bx}$ is shown in Fig. 3 (b). In the SBMF theory, the T_c is given as the lower one between the spinon-pairing temperature T_{pair} and the holon-BEC temperature T_{BEC} . The inset of Fig. 3 (b) displays $T_{\text{BEC}} \gg T_{\text{pair}}$, rendering $T_c = T_{\text{pair}}$ in the considered n_{bx} regime. Note that the T_c here is in the sense of Kosterlitz-Thouless transition. A comparison between Fig. 3 (b) and (a) suggests that T_c scales with $\tilde{\Delta}$, which is more clear when the $T_c \sim n_{bx}$ is well fitted by $0.42\tilde{\Delta} \sim n_{bx}$ for the d -wave and $0.9\tilde{\Delta} \sim n_{bx}$ for the s -wave in Fig. 3 (b), consistent with the Bardeen-Cooper-Schrieffer (BCS) theory. Inspiringly, for $n_{bx} \geq 0.75$, the $T_c \gtrsim 0.02t_{\parallel} \approx 80$ K, suggesting the HTSC in the liquid nitrogen temperature range.

On the above, we have adopted $\tilde{J}_{\perp} = \alpha J_{\perp}(1 - \delta_{tz})$ with $\alpha = 1$, where δ_{tz} denotes the hole density of the top- $3d_{z^2}$ orbital. For the reduced α , only the low- n_{bx} regime accommodating the interlayer s -wave pairing in Fig. 3 (a, b) shrinks but the high- n_{bx} regime accommodating the intralayer d -wave SC is not affected because the intralayer pairing is blind to \tilde{J}_{\perp} . Furthermore, assuming different ratios between the changes of the filling fractions of the two top-layer E_g orbitals turns out to yield similar results when expressed as functions of n_{bx} , as the dominant pairing under strong ε is the intra-bottom-layer pairing, which is blind to the filling fraction of the top layer. See the SI for details [157].

We have further employed the DMRG approach, which can capture the quantum fluctuation beyond mean-field, to compute the ground state of Hamiltonian (1) under different electric fields ε and the transferred electron-doping levels of the $d_{x^2-y^2}$ orbitals $\delta = n_{tx} + n_{bx} - 1$. For $\varepsilon = 0$, we have $\delta = 0$. When ε increases, it drives electrons from d_{z^2} -orbitals in the top layer to $d_{x^2-y^2}$ -orbitals in both layers, increasing δ . However, as the exact relationship between ε and δ is unclear, we set them as two independent variables in our DMRG study. The parameters t_{\parallel} and J_{\parallel} take the same values as the ones in the SBMF study while $\tilde{J}_{\perp} = 0.8J_{\parallel}$ is adopted in the DMRG study. To characterize the pairing symmetry and strength, we analyze the interlayer pairing correlation function $\Phi^{\perp}(r)$ and the intra-bottom-layer pairing correlation function $\Phi_b^{\parallel}(r)$. More details are provided in

METHODS.

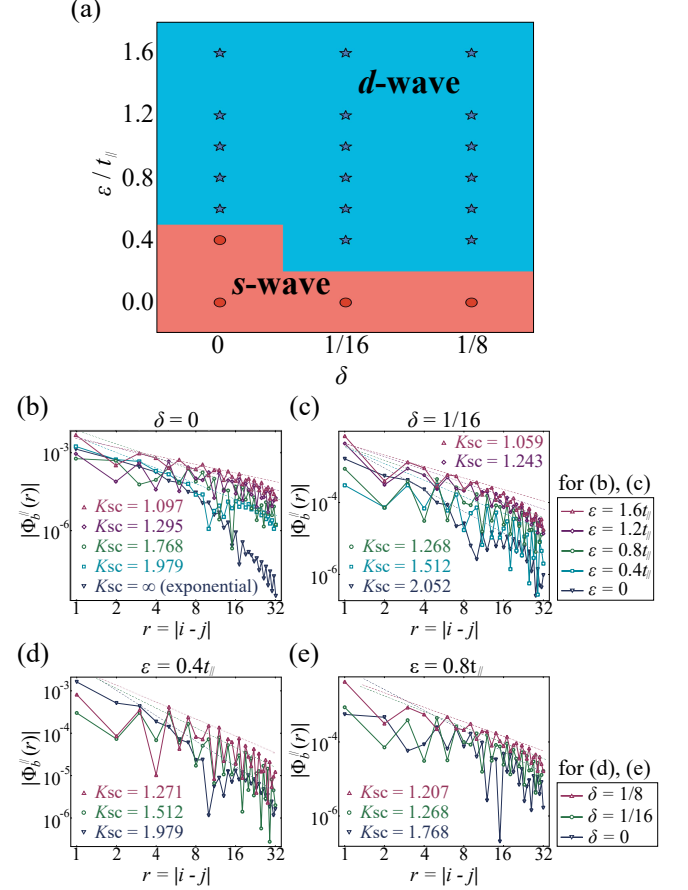


FIG. 4. The DMRG results. (a) The $\delta - \varepsilon$ phase diagram of the ground state. The red region corresponds to the s -wave pairing and the blue region to the d -wave pairing. (b)-(c) The absolute value of the intra-bottom-layer pairing correlation functions $|\Phi_b^{\parallel}(r)|$ under different electric fields $\varepsilon = 0, 0.4t_{\parallel}, 0.8t_{\parallel}, 1.2t_{\parallel}, 1.6t_{\parallel}$ for $\delta = 0$ in (b) and $\delta = 1/16$ in (c). (d)-(e) $|\Phi_b^{\parallel}(r)|$ for different transferred $d_{x^2-y^2}$ -electron-doping levels $\delta = 0, 1/16, 1/8$ under $\varepsilon = 0.4t_{\parallel}$ in (d) and $\varepsilon = 0.8t_{\parallel}$ in (e). The algebraic decay exponents K_{SC} are written in the four figures as well, reflecting the decay rate of the pairing correlation function with spatial distance, negatively correlated with the corresponding pairing strength. In (a-e), δ and ε are set as independent variables, since their exact relationship is unclear.

Fig. 4 (a) shows the pairing phase diagram with respect to δ ($= 0, 1/16, 1/8$) and ε ($\in [0, 1.6t_{\parallel}]$). Fig. 4 (b) shows the absolute value of the intra-bottom-layer pairing correlation functions $|\Phi_b^{\parallel}(r)|$ under different electric fields $\varepsilon = 0, 0.4t_{\parallel}, 0.8t_{\parallel}, 1.2t_{\parallel}, 1.6t_{\parallel}$ for $\delta = 0$, and the results for $\delta = 1/16$ are presented in Fig. 4 (c). It turns out that $|\Phi_b^{\parallel}(r)|$ exhibits algebraic decay under a non-zero external electric field with the decaying power exponent to be K_{SC} , i.e. $|\Phi_b^{\parallel}(r)| \propto r^{-K_{\text{SC}}}$ for large enough r , implying the presence of pairing within the bottom layers. Fig. 4 (d) and (e) depict $|\Phi_b^{\parallel}(r)|$ for different

transferred $d_{x^2-y^2}$ -electron-doping levels $\delta = 0, 1/16, 1/8$ under $\varepsilon = 0.4t_{\parallel}$ in (d) and $\varepsilon = 0.8t_{\parallel}$ in (e). All the algebraic decay exponents K_{SC} are provided accordingly.

The results indicate that (i) With the enhancement of the perpendicular electric field ε , and hence the transferred $d_{x^2-y^2}$ -electron-doping level δ , the pairing symmetry changes from interlayer s -wave to intra-bottom-layer d -wave (The criterion of the pairing symmetry is provided in **METHODS**); (ii) For all the transferred $d_{x^2-y^2}$ -electron-doping levels δ tested, the enhancement of the perpendicular electric field ε leads to a reduction of K_{SC} , suggesting the enhancement of the intra-bottom-layer pairing; (iii) Under all the perpendicular electric field strengths ε tested, the enhancement of the transferred $d_{x^2-y^2}$ -electron-doping level δ leads to a reduction of K_{SC} , suggesting the enhancement of the intra-bottom-layer pairing. From (ii) and (iii), it is clear that the enhancement of ε and hence δ will significantly enhance the intra-bottom-layer pairing. These results are quali-

tatively consistent with those of the SBMF study. More results are given in the SI [157].

Besides, we study the effect of interlayer Coulomb interaction. Our results show that the interlayer Coulomb interaction slightly promotes charge transfer between layers and the intra-bottom-layer pairing, while suppressing the interlayer pairing. See SI [157] for details.

The comprehensive two-orbital study

The above simplified single-orbital study has drawbacks: We cannot determine the relationship between the electron-doping of the $d_{x^2-y^2}$ orbitals and the electric field. In the SBMF study, we have to assume the ratio between the changes of the filling fractions of the two top-layer E_g orbitals. In addition, we do not know how the neglected $3d_{z^2}$ orbital degree of freedom affects the pairing nature. To settle these puzzles, we conduct a comprehensive two-orbital model [107] to study with,

$$\begin{aligned}
H = & -t_{\parallel} \sum_{\langle i,j \rangle, \mu} \hat{P} \left(c_{i\mu x\sigma}^{\dagger} c_{j\mu x\sigma} + \text{h.c.} \right) \hat{P} - t_{\perp} \sum_i \hat{P} \left(c_{itz\sigma}^{\dagger} c_{ibz\sigma} + \text{h.c.} \right) \hat{P} - t_{xz} \sum_{\langle i,j \rangle, \mu} \hat{P} \left(c_{i\mu x\sigma}^{\dagger} c_{j\mu z\sigma} + (z \leftrightarrow x) + \text{h.c.} \right) \hat{P} \\
& + J_{\parallel} \sum_{\langle i,j \rangle, \mu} \mathbf{S}_{i\mu x} \cdot \mathbf{S}_{j\mu x} + J_{\perp} \sum_i \mathbf{S}_{itz} \cdot \mathbf{S}_{ibz} + \tilde{J}_{\perp} \sum_i \mathbf{S}_{itx} \cdot \mathbf{S}_{ibx} + \epsilon_z \sum_{i\mu\sigma} n_{i\mu z\sigma} + \epsilon_x \sum_{i\mu\sigma} n_{i\mu x\sigma} \\
& + \frac{\varepsilon}{2} \sum_{i\alpha\sigma} n_{it\alpha\sigma} - \frac{\varepsilon}{2} \sum_{i\alpha\sigma} n_{ib\alpha\sigma}.
\end{aligned} \tag{2}$$

The operators $c_{i\mu\alpha\sigma}$, $n_{i\mu\alpha}$, $\mathbf{S}_{i\mu\alpha}$ take the same meanings as those in model (1) except for an extra index $\alpha = x/z$ labeling the orbital, and \hat{P} is a projection operator projecting out the double occupancy in the same orbital of all sites. Note that $\mathbf{S}_{i\mu\alpha}$ for each orbital is spin- $\frac{1}{2}$ operator. ϵ_{α} denotes the on-site energy of the orbital α . We adopt the tight-binding (TB) parameters reported in Ref. [141], i.e. $t_{\parallel} = 0.445$ eV, $t_{xz} = 0.221$ eV, $t_{\perp} = 0.503$ eV and $\epsilon_x - \epsilon_z = 0.367$ eV. The superexchange interactions are obtained through $J_{\parallel} \approx 4t_{\parallel}^2/U$ and $J_{\perp} \approx 4t_{\perp}^2/U$, with $U = 10t_{\parallel}$. Finally ε denotes the voltage between the two layers. Here, due to the weak super-exchange interaction between the d_{z^2} orbitals in the layer, we do not consider this term in our model. In addition, the Hund's coupling J_H of $\text{La}_3\text{Ni}_2\text{O}_7$ is generally considered to be in the range of 0.7 eV to 1 eV in past studies [68, 70, 76], which only slightly larger than the largest hopping parameter $t_{\perp} = 0.503$ eV and thus does not satisfy the premise of the Schrieffer-Wolf transformation or perturbation theory, we do not apply it here. More details are provided in **METHODS**.

Our SBMF results of Eq. (2) (see **METHODS** and the SI [157]) are shown in Fig. 5. Fig. 5(a) shows the ε -dependence of the hole densities $\delta_{\mu\alpha}$. Obviously, the δ_{tz}

enhances obviously with ε , suggesting that the top- $3d_{z^2}$ orbital is donating electrons. These donated electrons flow to the $3d_{x^2-y^2}$ orbitals in both layers, with more of them flowing to the bottom layer when $\varepsilon > 0.1$ eV while about half of them flow to the bottom layer when $\varepsilon \leq 0.1$ eV. Fig. 5(b) shows the ε -dependence of the pairing symmetry and the pairing gap amplitude of the bottom-layer $3d_{x^2-y^2}$ orbital. At low $\varepsilon \leq 0.03$ eV, the pairing symmetry is s -wave, whose pairing configuration is shown in Fig. 5(c), wherein the $3d_{z^2}$ -orbital form interlayer s -wave pseudo-gap, while the $3d_{x^2-y^2}$ orbital form s -wave SC with coexisting intralayer and interlayer pairing. In this regime the interlayer pairing is suppressed by the enhancement of ε while the intralayer pairing is enhanced. When $\varepsilon = 0$, the interlayer pairing gap is the largest. When ε is about 0.01 \sim 0.03 eV, the intralayer pairing gap is slightly larger than the interlayer pairing gap. When $\varepsilon > 0.03$ eV, the pairing symmetry is $d(3d_{x^2-y^2}) + is(3d_{z^2})$, whose pairing configuration is shown in Fig. 5(d). In this state, the $3d_{z^2}$ orbital form interlayer s -wave pseudo-gap, while the bottom-layer $3d_{x^2-y^2}$ orbital form intralayer d -wave SC. When ε enhances in this regime, the pairing amplitude for the d -wave part enhances promptly. For $\varepsilon > 0.13$ eV, the

pairing amplitude can go beyond 0.02 eV. Then from the relation $T_c \approx 0.42\tilde{\Delta}$ for the d -wave SC illustrated in Fig. 3(b), we have got HTSC with $T_c \gtrsim 80$ K!

The result shown in Fig. 5(b) for the comprehensive two-orbital study and that shown in Fig. 3(b) for the simplified one-orbital study look similar, except that in Fig. 5(b) the result is expressed as function of the directly controllable quantity ε . Actually, if we replace the x -axis of Fig. 5(b) by the calculated $n_{bx} = 1 - \delta_{bx}$, the resulting curve nearly coincides with Fig. 3(b), particularly in the large- n_{bx} regime, see the SI [157]. The main reason for such similarity lies in that under strong ε , the dominant superconducting pairing is the intra-bottom-layer $3d_{x^2-y^2}$ -orbital pairing, which is insensitive to the $3d_{z^2}$ orbital. The main new information obtained in the two-orbital study lies in that the $3d_{z^2}$ orbital form interlayer s -wave pseudo-gap which is mixed with the intra-bottom-layer d -wave HTSC of the $3d_{x^2-y^2}$ orbital in the ratio of 1 : i, as shown in Fig. 5(d). This state breaks time-reversal symmetry, although the experimentally detected superconducting gap is the standard d -wave gap of the $3d_{x^2-y^2}$ orbital. This intriguing result is left for experimental verification.

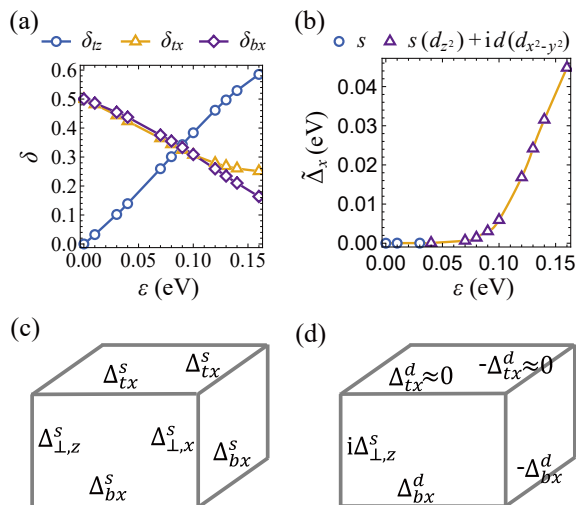


FIG. 5. The SBMF results for the two-orbital model. (a) The hole densities $\delta_{\mu\alpha}$ for the three orbitals as functions of the strength of the electric field ε . (b) The pairing gap amplitude of the bottom-layer $3d_{x^2-y^2}$ -orbital as function of ε . (c)-(d) The pairing configurations of the s -wave and the $d(3d_{x^2-y^2}) + is(3d_{z^2})$ -wave, respectively.

DISCUSSION

In conclusion, we propose that an imposed strong perpendicular electric field can drive HTSC with T_c above the boiling point of liquid nitrogen in the single-bilayer film of $\text{La}_3\text{Ni}_2\text{O}_7$ at AP. The reason lies in that under the strong electric field, the electrons in the layer with

higher potential energy will flow to the layer with lower potential energy, to fill the $3d_{x^2-y^2}$ orbitals in the latter layer. When the imposed electric field is weak, it acts as the “pseudo-Zeeman field” operating on the layer index which suppresses the interlayer SC, possibly inducing the PDW state. With considerably enhanced filling fraction, the $3d_{x^2-y^2}$ electrons in that layer just mimic the cuprates, which form intralayer d -wave HTSC with strongly enhanced T_c . Our combined one-orbital and two-orbital studies consistently verify this idea.

Presently, while different groups have provided slightly different TB parameters for the $\text{La}_3\text{Ni}_2\text{O}_7$ ultrathin film grown on SLAO substrate at AP, we have just adopted one set of these TB parameters to perform our calculations. However, the strong-coupling calculations performed here do not seriously rely on the accurate values of these parameters, because the main physics here is clear and simple. Actually, the well consistency between the result of the comprehensive two-orbital study and those of the simplified one-orbital studies with assuming different input conditions just verifies the robustness of our conclusion.

Moreover, we want to emphasize that the essence of introducing the perpendicular electric field is breaking the symmetry of the two layers by making their filling fractions different to each other. Actually, the filling fractions of different NiO layers in the $\text{La}_3\text{Ni}_2\text{O}_7$ ultrathin film grown on the SLAO substrate may differ from each other because of the existence of the substrate on one side of the film. This can be considered as effective electric field. Thus, our work provides a possible way to understand the high T_c of the $\text{La}_3\text{Ni}_2\text{O}_7$ ultrathin film grown on the SLAO substrate.

METHODS

The one-orbital model

The SBMF theory is used to solve the one-orbital model (1). In the SBMF approach, the superexchange terms are decomposed in $\chi - \Delta$ channel, e.g. $\mathbf{S}_{it} \cdot \mathbf{S}_{ib} = -\frac{3}{8} (\langle \chi^{\dagger\dagger} \rangle \chi_i^\dagger + \text{h.c.} + \langle \Delta^{\dagger\dagger} \rangle \Delta_i^\dagger + \text{h.c.})$, χ and Δ represents hopping and pairing operators respectively. These MF parameters are further solved in a self-consistent manner. The specific steps can be referenced from prior work [79, 107, 156] and SI [157].

We also employ the DMRG method [158, 159] to solve the ground state of the Hamiltonian (1) as a comparison for the SBMF approach. The tensor libraries TensorKit [160] and FiniteMPS [161] provide an implementation of the required symmetry [162, 163]. We study the model on a $2 \times 2 \times L_x$ lattice with the open boundary conditions in the x direction and choose $L_x = 64$ for calculations. The matrix product state is constructed as shown in Fig. 6. We keep up to $D = 12000 U(1)_{\text{charge}} \times \text{SU}(2)_{\text{spin}}$ mul-

triplets in DMRG simulations and ensure the convergence accuracy of 10^{-6} .

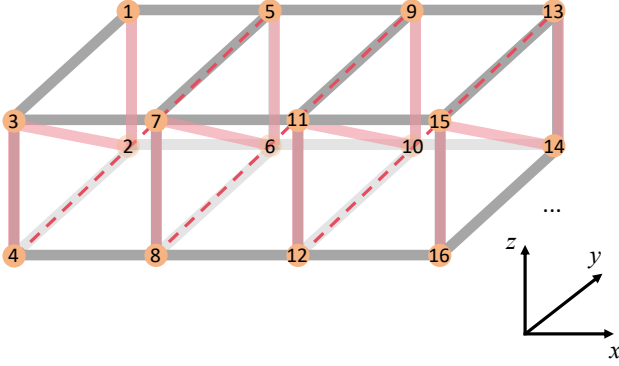


FIG. 6. Illustration of the zigzag path in DMRG calculation.

The interlayer and intralayer singlet pairing operators take the form of

$$\begin{aligned}\Delta_i^{\perp\dagger} &= \frac{1}{\sqrt{2}} \left(c_{i\uparrow}^\dagger c_{ib\downarrow}^\dagger - c_{it\downarrow}^\dagger c_{ib\uparrow}^\dagger \right), \\ \Delta_{i\mu}^{\parallel\dagger} &\equiv \Delta_{i\mu}^{\mathbf{x}\dagger} = \frac{1}{\sqrt{2}} \left(c_{i\mu\uparrow}^\dagger c_{i+\mathbf{x},\mu\downarrow}^\dagger - c_{i\mu\downarrow}^\dagger c_{i+\mathbf{x},\mu\uparrow}^\dagger \right), \\ \Delta_{i\mu}^{\mathbf{y}\dagger} &= \frac{1}{\sqrt{2}} \left(c_{i\mu\uparrow}^\dagger c_{i+\mathbf{y},\mu\downarrow}^\dagger - c_{i\mu\downarrow}^\dagger c_{i+\mathbf{y},\mu\uparrow}^\dagger \right).\end{aligned}\quad (3)$$

Here, the subscripts $i + \mathbf{x}$ ($i + \mathbf{y}$) represent the NN site of the site \mathbf{i} in the x (y) direction. Fig. 7 shows how the singlet pairing operators are defined.

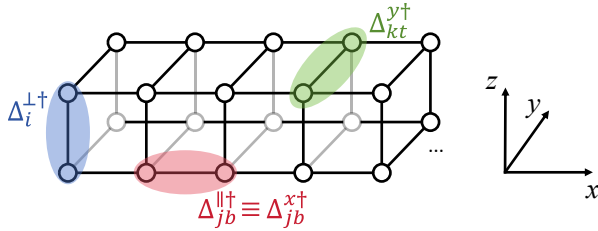


FIG. 7. Illustration of the singlet pairing operators $\Delta_i^{\perp\dagger}$, $\Delta_{i\mu}^{\parallel\dagger}$ and $\Delta_{i\mu}^{\mathbf{y}\dagger}$.

The considered correlation functions are defined as follow

$$\begin{aligned}\Phi^\perp(r) &= \langle \Delta_i^{\perp\dagger} \Delta_j^\perp \rangle, \\ \Phi_\mu^\parallel(r) &\equiv \Phi_\mu^{\mathbf{x}\mathbf{x}}(r) = \langle \Delta_{i\mu}^{\parallel\dagger} \Delta_{j\mu}^\parallel \rangle, \\ \Phi_\mu^{\mathbf{x}\mathbf{y}}(r) &= \langle \Delta_{i\mu}^{\parallel\dagger} \Delta_{j\mu}^{\mathbf{y}} \rangle,\end{aligned}\quad (4)$$

where $r = |\mathbf{i} - \mathbf{j}|$ is the distance between the sites i and j .

For a pairing channel whose absolute value of correlation function decays algebraically with distance, following the form $r^{-K_{SC}}$, the decay exponent K_{SC} is associated with the Luttinger parameter specific to the channel.

$K_{SC} < 2$ signals a divergent superconducting susceptibility in that channel. The channel with the lowest K_{SC} value is considered to dominate the pairing behavior.

The dominant pairing channel is related to pairing symmetry. For the case where interlayer pairing dominates, the pairing symmetry is restricted to s -wave pairing; while for the case where intralayer pairing in the bottom-layer dominates, we determine the pairing symmetry by the sign function $\text{sgn}[\Phi_b^\parallel(r)\Phi_b^{\mathbf{x}\mathbf{y}}(r)]$. If $\text{sgn}[\Phi_b^\parallel(r)\Phi_b^{\mathbf{x}\mathbf{y}}(r)] = -1$ holds for all r , the ground state can be identified as the d -wave pairing SC state. See SI [157] for more details on DMRG.

The two-orbital model

Here we provide more technique details for the SBMF study on the two-orbital model (2). The electron operator is decomposed as $c_{i\mu\alpha}^\dagger = f_{i\mu\alpha}^\dagger b_{i\mu\alpha}$, where f is spinon operator and b is holon operator. Since we have found that $T_{BEC} \gg T_{\text{pair}}$ in the considered n_{bx} regime and T_{pair} is proportional to the zero-temperature spinon pairing gap, we can get the critical temperature of superconductivity only by calculating the ground-state spinon pairing gap. Thus we only consider the spinon Hamiltonian at zero temperature. The superexchange term is also decomposed in $\chi - \Delta$ channel. The spinon Hamiltonian is described as

$$\begin{aligned}H_{\text{spinon}} &= -t_{\parallel} \sum_{\langle i,j \rangle, \mu} \delta_{\mu\mathbf{x}} \left(f_{i\mu\mathbf{x}\sigma}^\dagger f_{j\mu\mathbf{x}\sigma} + \text{h.c.} \right) \\ &\quad - t_{xz} \sqrt{\delta_{tx}\delta_{tz}} \sum_{\langle i,j \rangle} \left(f_{it\mathbf{x}\sigma}^\dagger f_{jt\mathbf{z}\sigma} + f_{it\mathbf{z}\sigma}^\dagger f_{jt\mathbf{x}\sigma} + \text{h.c.} \right) \\ &\quad - \frac{3}{8} J_{\parallel} \sum_{\langle i,j \rangle, \mu} \left(\chi_{ij,\mu\mathbf{x}}^\dagger \langle \chi_{\mu\mathbf{x}} \rangle + \text{h.c.} - \langle \chi_{\mu\mathbf{x}}^\dagger \rangle \langle \chi_{\mu\mathbf{x}} \rangle \right) \\ &\quad - \frac{3}{8} J_{\parallel} \sum_{\langle i,j \rangle, \mu} \left(\Delta_{ij,\mu\mathbf{x}}^\dagger \langle \Delta_{\mu\mathbf{x}} \rangle + \text{h.c.} - \langle \Delta_{\mu\mathbf{x}}^\dagger \rangle \langle \Delta_{\mu\mathbf{x}} \rangle \right) \\ &\quad - \frac{3}{8} J_{\perp} \sum_i \left(\chi_{iz}^\dagger \langle \chi_z^\perp \rangle + \text{h.c.} - \langle \chi_z^{\perp\dagger} \rangle \langle \chi_z^\perp \rangle \right) \\ &\quad - \frac{3}{8} J_{\perp} \sum_i \left(\Delta_{iz}^\dagger \langle \Delta_z^\perp \rangle + \text{h.c.} - \langle \Delta_z^{\perp\dagger} \rangle \langle \Delta_z^\perp \rangle \right) \\ &\quad - \frac{3}{8} \tilde{J}_{\perp} \sum_i \left(\Delta_{ix}^\dagger \langle \Delta_x^\perp \rangle + \text{h.c.} - \langle \Delta_x^{\perp\dagger} \rangle \langle \Delta_x^\perp \rangle \right) \\ &\quad + \sum_{i\mu\alpha\sigma} \epsilon_\alpha n_{i\mu\alpha\sigma} + \frac{\varepsilon}{2} \sum_{i\alpha\sigma} n_{it\alpha\sigma} - \frac{\varepsilon}{2} \sum_{i\alpha\sigma} n_{ib\alpha\sigma}.\end{aligned}\quad (5)$$

where $\delta_{\mu\alpha} = \langle b_{i\mu\alpha} b_{j\mu\alpha}^\dagger \rangle$ since holon condense at zero temperature. Under the electric field, we have $\delta_{bz} = 0$ and δ_{tz} , δ_{tx} and δ_{bx} are solved in a self-consistent manner by adjustment to onsite energies ϵ_α (See SI [157] for

more details). The mean-field order parameters are represented by

$$\begin{aligned}
\chi_{ij,\mu x} &= \sum_{\sigma} f_{i\mu x\sigma}^{\dagger} f_{j\mu x\sigma}, \\
\chi_{iz}^{\perp\dagger} &= \sum_{\sigma} f_{izt\sigma}^{\dagger} f_{izb\sigma}, \\
\Delta_{ij,\mu\alpha}^{\dagger} &= f_{i\mu\alpha\uparrow}^{\dagger} f_{j\mu\alpha\downarrow}^{\dagger} - f_{i\mu\alpha\downarrow}^{\dagger} f_{j\mu\alpha\uparrow}^{\dagger}, \\
\Delta_{i\alpha}^{\perp\dagger} &= f_{it\alpha\uparrow}^{\dagger} f_{ib\alpha\downarrow}^{\dagger} - f_{ib\alpha\downarrow}^{\dagger} f_{it\alpha\uparrow}^{\dagger},
\end{aligned} \tag{6}$$

and

$$\begin{aligned}
\chi_{\mu x} &= \frac{1}{2N} \sum_{\langle i,j \rangle} \chi_{ij,\mu x}, \quad \chi_z^{\perp} = \frac{1}{N} \sum_i \chi_{iz}^{\perp}, \\
\Delta_{\mu x}^{\mathbf{x}} &= \frac{1}{2N} \sum_{\langle i,j \rangle} \Delta_{ij,\mu x}, \quad \Delta_{\alpha}^{\perp} = \frac{1}{N} \sum_i \Delta_{i\alpha}^{\perp}.
\end{aligned} \tag{7}$$

Notably, the spin-exchange \tilde{J}_{\perp} of the Hamiltonian in Eq. (2) doesn't produce a hopping term χ_x^{\perp} in Eq. (5), which is the feature of such a bilayer system. Without interlayer hopping, a small interlayer spin-exchange J_{\perp} leads to $\langle \chi^{\perp} \rangle \approx 0$.

Consequently, the $3d_{z^2}$ orbital only participate in the interlayer pairing. However, this pairing is not SC as the corresponding SC order parameter goes to zero in the SBMF theory due to $\delta_{bz} = 0$. The SC is carried by the $3d_{x^2-y^2}$ orbitals, which can form both intralayer and interlayer pairing. The superconducting T_c scales with the ground state gap amplitude of the $3d_{x^2-y^2}$ orbitals via the BCS relation exhibited in Fig. 3(b).

The expectation value of the mean-field order parameters are obtained by numerically solving the following self-consistent equations

$$\begin{aligned}
\delta_{\mu\alpha} &= 1 - \frac{1}{N} \sum_k \left(\langle f_{k\mu\alpha\uparrow}^{\dagger} f_{k\mu\alpha\uparrow} \rangle + \langle f_{-k\mu\alpha\downarrow}^{\dagger} f_{-k\mu\alpha\downarrow} \rangle \right), \\
\delta_{tz} &= 0, \quad \sum_{\mu\alpha} \delta_{\mu\alpha} = 1, \\
\langle \chi_{\mu x} \rangle &= \frac{1}{N} \sum_k \epsilon(\mathbf{k}) \left(\langle f_{k\mu x\uparrow}^{\dagger} f_{k\mu x\uparrow} \rangle + \langle f_{-k\mu x\downarrow}^{\dagger} f_{-k\mu x\downarrow} \rangle \right), \\
\langle \chi_z^{\perp} \rangle &= \frac{1}{N} \sum_k \left(\langle f_{ktz\uparrow}^{\dagger} f_{kbz\uparrow} \rangle + \langle f_{-ktz\downarrow}^{\dagger} f_{-kbz\downarrow} \rangle \right), \\
\langle \Delta_{\mu x}^{\mathbf{x}} \rangle^* &= \frac{1}{N} \sum_k 2 \cos(k_x) \langle f_{k\mu x\uparrow}^{\dagger} f_{-k\mu x\downarrow}^{\dagger} \rangle, \\
\langle \Delta_{\alpha}^{\perp} \rangle^* &= \frac{2}{N} \sum_k \langle f_{kt\alpha\uparrow}^{\dagger} f_{-kb\alpha\downarrow}^{\dagger} \rangle,
\end{aligned} \tag{8}$$

where $\epsilon(\mathbf{k}) = \frac{\cos(k_x) + \cos(k_y)}{2}$.

DATA AVAILABILITY

The data generated in this study have been deposited in the Zenodo database at <https://zenodo.org/records/17691236>.

CODE AVAILABILITY

The code that supports the plots within this paper is available from the corresponding author upon request.

ACKNOWLEDGEMENT

We are grateful to the stimulating discussions with Chen Lu. F. Y. and C. W. is supported by the National Natural Science Foundation of China (NSFC) under the Grant No. 12234016. F. Y. is also supported by the CAS Superconducting Research Project under Grant No. [SCZX-0101] and the NSFC under the Grant No. 12074031. C. W. is also supported by the NSFC under the Grant No. 12174317. D. X. Y. is supported by NSFC-12494591, NSFC-92165204, NSFC-92565303, NKRDP-2022YFA1402802, Research Center for Magnetoelectric Physics of Guangdong Province (2024B0303390001), and Guangdong Provincial Quantum Science Strategic Initiative (GDZX2401010). C. W. is also supported by the New Cornerstone Science Foundation.

AUTHOR CONTRIBUTIONS

F. Yang proposed the main idea and supervised the study. Z.-Y. Shao performed the SBMF study. J.-H. Ji performed the DMRG study. D.-X. Yao and C. Wu helped shape the main idea. F. Yang, Z.-Y. Shao and J.-H. Ji wrote the paper.

ADDITIONAL INFORMATION

Competing Interests The authors declare no competing interests.

SUPPLEMENTARY INFORMATION

A. SLAVE-BOSON MEAN-FIELD TREATMENT OF THE ONE-ORBITAL MODEL

In the one-orbital model, we begin with the Hamiltonian

$$H = -t_{\parallel} \sum_{\langle i,j \rangle, \mu, \sigma} \hat{P} \left(c_{i\mu\sigma}^{\dagger} c_{j\mu\sigma} + \text{h.c.} \right) \hat{P} + \sum_{i, \mu} \epsilon_{\mu} n_{i\mu} + J_{\parallel} \sum_{\langle i,j \rangle, \mu} \mathbf{S}_{i\mu} \cdot \mathbf{S}_{j\mu} + \tilde{J}_{\perp} \sum_i \mathbf{S}_{it} \cdot \mathbf{S}_{ib}, \quad (\text{S1})$$

where $c_{i\mu\sigma}^{\dagger}$ creates a electron in the $d_{x^2-y^2}$ orbital with the spin $\sigma = \{\uparrow, \downarrow\}$ at the lattice site i in the layer $\mu = \{t, b\}$. $n_{i\mu} = \sum_{\sigma} c_{i\mu\sigma}^{\dagger} c_{i\mu\sigma}$ is the particle number operator. $\mathbf{S}_{i\mu} = \frac{1}{2} c_{i\mu\sigma}^{\dagger} [\sigma]_{\sigma\sigma'} c_{i\mu\sigma'}$ is the spin operator with Pauli matrix $\sigma = (\sigma_x, \sigma_y, \sigma_z)$. \hat{P} is a projection operator projecting out the double occupancy of all site. Here we set $t_{\parallel} = 1$ as the unit, and the intralayer and interlayer spin exchange are given by $J_{\parallel} = 0.4t_{\parallel}$ and $\tilde{J}_{\perp} \approx \alpha J_{\perp} (1 - \delta_{tz})$ with $J_{\perp} = 1.3J_{\parallel}$ and $\alpha = 1$, where δ_{tz} denotes the hole density of the top- $3d_{z^2}$ orbital. The particle number of the bottom-layer d_{z^2} orbital is near half-filling without external electric field, thus in the strong-coupling limit, the bottom-layer d_{z^2} orbital approaches half-filling and becomes incapable of accommodating additional electrons, even under a small perpendicular electric field. Therefore we fix the particle number of the bottom-layer d_{z^2} orbital $n_{bz} = 1$. Considering that the electrons flow from the top layer only to the bottom layer $d_{x^2-y^2}$ orbital, we express the particle number of the top-layer d_{z^2} orbital, the top-layer $d_{x^2-y^2}$ orbital and the bottom layer $d_{x^2-y^2}$ orbital as $n_{tz} = 1 - \delta$, $n_{tx} = 0.5 - \eta_1$ and $n_{bx} = 0.5 + \delta + \eta_1 = 0.5 + \eta_2$ respectively. In this simplified single-orbital study, we cannot determine the concrete relation between ε and δ or $\eta_{1,2}$. But clearly, δ and η_1 enhance with the enhancement of ε . Thus we set δ and η_1 as certain numbers and ϵ_{μ} corresponding to chemical potential is consistently derived from δ , then $\varepsilon = \epsilon_t - \epsilon_b$.

To get the knowledge of η_1/δ in different perpendicular electric field, we solve the tight-binding (TB) Hamiltonian with TB parameters reported in Ref. [141], i.e. $t_{\parallel} = 0.445$ eV, $t_{xz} = 0.221$ eV, $t_{\perp} = 0.503$ eV and $\epsilon_x - \epsilon_z = 0.367$ eV, and an additional external electric field term $(\varepsilon/2) \sum_{i, \alpha, \sigma} (n_{it\alpha\sigma} - n_{ib\alpha\sigma})$. We plot the (δ, η_1) points (Fig. A1), finding that $\eta_1/\delta \approx 1/2$. Thus we assume $\eta_1/\delta = 1/2$ (i.e. $(n_{tx} - 0.5)/(n_{bx} - 0.5) = -\eta_1/\eta_2 = -1/3$) in the one-orbital model study.

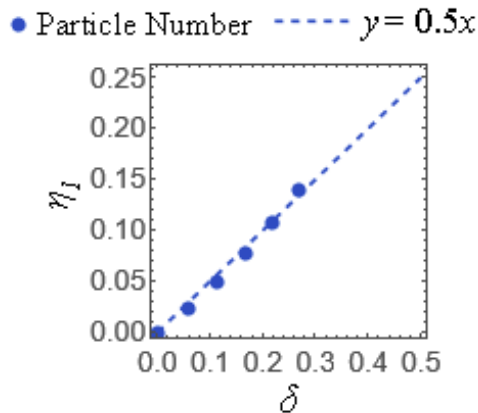


FIG. A1. The change of electron number δ and η_1 under different electric field. The results are represented by the dots (δ, η_1) . All of the dots are near the $y = 0.5x$ line (dashed line), indicating that $\eta_1 \approx 0.5\delta$.

We solve the Hamiltonian in Eq. (S1) by slave-boson mean-field (SBMF) theory [156]. The electron operator (c) is decomposed into the product of a fermionic spinon operator (f) and a bosonic holon operator (b), i.e. $c_{i\mu\sigma}^{\dagger} = f_{i\mu\sigma}^{\dagger} b_{i\mu}$. Then the electron pairing operator is expressed as

$$\Delta_e \equiv cc = b^{\dagger} b^{\dagger} f f, \quad (\text{S2})$$

and the expectation value is the product of the expectation value of the holon operators and the one of the spinon pairing operator (defined as $\Delta \equiv ff$),

$$\langle \Delta_e \rangle = \langle b^{\dagger} b^{\dagger} \rangle \langle f f \rangle. \quad (\text{S3})$$

When the temperature is below the holon condensation temperature T_{BEC} , holons condense and $\langle b \rangle = \langle b^\dagger \rangle = \sqrt{\delta}$, where δ is the hole density, while $\langle b \rangle = \langle b^\dagger \rangle = 0$ when the temperature is above T_{BEC} .

$$\langle b \rangle = \langle b^\dagger \rangle = \begin{cases} \sqrt{\delta}, & T < T_{\text{BEC}} \\ 0, & T > T_{\text{BEC}} \end{cases} \quad (\text{S4})$$

The spinon pairing operator $\Delta \equiv ff$ has a non-zero expectation value when the temperature is below the spinon pairing temperature T_{pair} while the expectation value is zero when the temperature is above T_{pair} .

$$\langle \Delta \rangle = \langle ff \rangle \begin{cases} > 0, & T < T_{\text{pair}} \\ = 0, & T > T_{\text{pair}} \end{cases} \quad (\text{S5})$$

Thus, the electron pairing operator Δ_e has a non-zero expectation value if and only if both $\langle b^\dagger b^\dagger \rangle$ and $\langle \Delta \rangle$ are non-zero, i.e. if and only if the temperature is below both T_{BEC} and T_{pair} . Therefore, the critical temperature of superconductivity (SC), T_c , is the lower one between T_{BEC} and T_{pair} ,

$$T_c = \min(T_{\text{BEC}}, T_{\text{pair}}). \quad (\text{S6})$$

The method for determining T_{pair} and T_{BEC} is given below. For the doping level considered in this work, $T_{\text{BEC}} \sim 10^3 \text{ K} \gg T_{\text{pair}}$ (see the main text), therefore $T_c = T_{\text{pair}}$.

The mean-field Hamiltonian of spinon and holon can be expressed as

$$\begin{aligned} H_{\text{spinon}} = & -t_{\parallel} \sum_{\langle i,j \rangle, \mu, \sigma} \left(\langle b_{i\mu} b_{j\mu}^\dagger \rangle f_{i\mu\sigma}^\dagger f_{j\mu\sigma} + \text{h.c.} \right) + \sum_{i, \mu, \sigma} \epsilon_{\mu} f_{i\mu\sigma}^\dagger f_{i\mu\sigma} \\ & - \frac{3}{8} J_{\parallel} \sum_{\langle i,j \rangle, \mu} \left(\langle \chi_{\mu}^\dagger \rangle \chi_{ij, \mu} + \text{h.c.} + \langle \Delta_{\mu}^\dagger \rangle \Delta_{ij, \mu} + \text{h.c.} - \langle \chi_{\mu}^\dagger \rangle \langle \chi_{\mu} \rangle - \langle \Delta_{\mu}^\dagger \rangle \langle \Delta_{\mu} \rangle \right) \\ & - \frac{3}{8} (1 - \delta) J_{\perp} \sum_i \left(\langle \chi^{\perp\dagger} \rangle \chi_i^{\perp} + \text{h.c.} + \langle \Delta^{\perp\dagger} \rangle \Delta_i^{\perp} + \text{h.c.} - \langle \chi^{\perp\dagger} \rangle \langle \chi^{\perp} \rangle - \langle \Delta^{\perp\dagger} \rangle \langle \Delta^{\perp} \rangle \right), \end{aligned} \quad (\text{S7})$$

and

$$H_{\text{holon}} = -t_{\parallel} \sum_{\langle i,j \rangle, \mu} \left(\langle \chi_{ij, \mu} \rangle b_{i\mu}^\dagger b_{j\mu} + \text{h.c.} \right), \quad (\text{S8})$$

where $\langle b_{i\mu} \rangle = \langle b_{i\mu}^\dagger \rangle = \sqrt{\delta_{\mu}}$ is sustained below the holon condensation temperature, and the bonding and pairing order parameters are defined as

$$\begin{aligned} \chi_{ij, \mu}^\dagger &= \sum_{\sigma} f_{i\mu\sigma}^\dagger f_{j\mu\sigma}, \quad \chi_{\mu}^\dagger = \frac{1}{2N} \sum_{\langle i,j \rangle} \chi_{ij, \mu}^\dagger, \\ \chi_i^{\perp\dagger} &= \sum_{\sigma} f_{it\sigma}^\dagger f_{ib\sigma}, \quad \chi^{\perp\dagger} = \frac{1}{N} \sum_i \chi_i^{\perp\dagger}, \\ \Delta_{ij, \mu}^\dagger &= f_{i\mu\uparrow}^\dagger f_{j\mu\downarrow}^\dagger - f_{i\mu\downarrow}^\dagger f_{j\mu\uparrow}^\dagger, \quad \Delta_{\mu}^{\mathbf{x}(\mathbf{y})} = \frac{1}{2N} \sum_{\mathbf{R}_i - \mathbf{R}_j = \pm \mathbf{x}(\mathbf{y})} \Delta_{ij, \mu}, \\ \Delta_i^{\perp\dagger} &= f_{it\uparrow}^\dagger f_{ib\downarrow}^\dagger - f_{it\downarrow}^\dagger f_{ib\uparrow}^\dagger, \quad \Delta^{\perp} = \frac{1}{N} \sum_i \Delta_i^{\perp}. \end{aligned} \quad (\text{S9})$$

Here, N is site number and \mathbf{x}/\mathbf{y} is the basis vector along the $+x/y$ direction.

In the mean-field approach, we constrain the particle number and obtain the expectation value of the mean-field

order parameters by solving the self-consistent equations derived from Eq. (S7).

$$\begin{aligned}
\delta_\mu &= 1 - \frac{1}{N} \sum_k \left(\langle f_{k\mu\uparrow}^\dagger f_{k\mu\uparrow} \rangle + \langle f_{-k\mu\downarrow}^\dagger f_{-k\mu\downarrow} \rangle \right), \quad \delta_t = 0.5 + \eta_1, \quad \delta_b = 0.5 - \eta_2, \\
\langle \chi_\mu \rangle &= \frac{1}{2N} \sum_{\langle i,j \rangle} \langle \chi_{ij,\mu} \rangle = \frac{1}{N} \sum_k \frac{\cos(k_x) + \cos(k_y)}{2} \left(\langle f_{k\mu\uparrow}^\dagger f_{k\mu\uparrow} \rangle + \langle f_{-k\mu\downarrow}^\dagger f_{-k\mu\downarrow} \rangle \right), \\
\langle \chi^\perp \rangle &= \frac{1}{N} \sum_i \langle \chi_i^\perp \rangle = \frac{1}{N} \sum_k \left(\langle f_{kt\uparrow}^\dagger f_{kb\uparrow} \rangle + \langle f_{-kt\downarrow}^\dagger f_{-kb\downarrow} \rangle \right), \\
\langle \Delta_\mu^{\mathbf{x}(\mathbf{y})} \rangle^* &= \frac{1}{2N} \sum_{\mathbf{R}_i - \mathbf{R}_j = \pm \mathbf{x}(\mathbf{y})} \langle \Delta_{ij,\mu} \rangle^* = \frac{1}{N} \sum_k 2 \cos(k_{x(\mathbf{y})}) \langle f_{k\mu\uparrow}^\dagger f_{-k\mu\downarrow}^\dagger \rangle, \\
\langle \Delta^\perp \rangle^* &= \frac{1}{N} \sum_i \langle \Delta_i^\perp \rangle^* = \frac{2}{N} \sum_k \langle f_{kt\uparrow}^\dagger f_{-kb\downarrow}^\dagger \rangle.
\end{aligned} \tag{S10}$$

Here, $f_{\mathbf{k}\mu\sigma} = \frac{1}{\sqrt{N}} \sum_i f_{i\mu\sigma} e^{-i\mathbf{k}\cdot\mathbf{R}_i}$, $k_{x/y}$ is the x/y -component of \mathbf{k} , and $\langle \Delta_\mu^{\mathbf{x}/\mathbf{y}} \rangle$ is the gap of the nearest neighbor bond along the x/y direction. For s -wave pairing, $\langle \Delta_\mu^{\mathbf{y}} \rangle = \langle \Delta_\mu^{\mathbf{x}} \rangle$. For d -wave pairing, $\langle \Delta_\mu^{\mathbf{y}} \rangle = -\langle \Delta_\mu^{\mathbf{x}} \rangle$.

In the self consistent equations, the expectation values of the operators are obtained as follows. The matrix form of the spinon Hamiltonian is

$$H_{\text{spinon}} = \sum_k \begin{pmatrix} f_{kt\uparrow}^\dagger & f_{kb\uparrow}^\dagger & f_{-kt\downarrow} & f_{-kb\downarrow} \end{pmatrix} \begin{pmatrix} H_\chi(\mathbf{k}) & H_\Delta(\mathbf{k}) \\ H_\Delta^\dagger(\mathbf{k}) & -H_\chi^T(\mathbf{k}) \end{pmatrix} \begin{pmatrix} f_{kt\uparrow} \\ f_{kb\downarrow} \\ f_{-kt\downarrow} \\ f_{-kb\downarrow}^\dagger \end{pmatrix}, \tag{S11}$$

where

$$\begin{aligned}
H_\chi(\mathbf{k}) &= \begin{pmatrix} -2(t_\parallel \delta_t + \frac{3}{8} J_\parallel \langle \chi_t \rangle) (\cos(k_x) + \cos(k_y)) + \epsilon_t & -\frac{3}{8} (1 - \delta) J_\perp \langle \chi^\perp \rangle \\ -\frac{3}{8} (1 - \delta) J_\perp \langle \chi^\perp \rangle & -2(t_\parallel \delta_b + \frac{3}{8} J_\parallel \langle \chi_b \rangle) (\cos(k_x) + \cos(k_y)) + \epsilon_b \end{pmatrix}, \\
H_\Delta(\mathbf{k}) &= \begin{pmatrix} -\frac{3}{4} J_\parallel (\langle \Delta_t^{\mathbf{x}} \rangle \cos(k_x) + \langle \Delta_t^{\mathbf{y}} \rangle \cos(k_y)) & -\frac{3}{8} (1 - \delta) J_\perp \langle \Delta^\perp \rangle \\ -\frac{3}{8} (1 - \delta) J_\perp \langle \Delta^\perp \rangle & -\frac{3}{4} J_\parallel (\langle \Delta_b^{\mathbf{x}} \rangle \cos(k_x) + \langle \Delta_b^{\mathbf{y}} \rangle \cos(k_y)) \end{pmatrix}.
\end{aligned} \tag{S12}$$

H_{spinon} can be diagonalized by a Bogoliubov transformation.

$$H_{\text{spinon}} = \sum_k \begin{pmatrix} \gamma_{k1}^\dagger & \gamma_{k2}^\dagger & \gamma_{k3}^\dagger & \gamma_{k4}^\dagger \end{pmatrix} \text{diag}(E_{k1}, E_{k2}, E_{k3}, E_{k4}) \begin{pmatrix} \gamma_{k1} \\ \gamma_{k2} \\ \gamma_{k3} \\ \gamma_{k4} \end{pmatrix}, \tag{S13}$$

where

$$\xi^\dagger(\mathbf{k}) \begin{pmatrix} H_\chi(\mathbf{k}) & H_\Delta(\mathbf{k}) \\ H_\Delta^\dagger(\mathbf{k}) & -H_\chi^T(\mathbf{k}) \end{pmatrix} \xi(\mathbf{k}) = \text{diag}(E_{k1}, E_{k2}, E_{k3}, E_{k4}), \quad \begin{pmatrix} f_{kt\uparrow} \\ f_{kb\uparrow} \\ f_{-kt\downarrow} \\ f_{-kb\downarrow}^\dagger \end{pmatrix} = \xi(\mathbf{k}) \begin{pmatrix} \gamma_{k1} \\ \gamma_{k2} \\ \gamma_{k3} \\ \gamma_{k4} \end{pmatrix}. \tag{S14}$$

Here, γ is fermionic operator, whose expectation value is

$$\langle \gamma_{km}^\dagger \gamma_{k'n} \rangle = \delta_{kk'} \delta_{mn} n_F(E_{km}), \quad \langle \gamma_{km} \gamma_{k'n} \rangle = \langle \gamma_{km}^\dagger \gamma_{k'n}^\dagger \rangle = 0, \tag{S15}$$

where $m = 1, 2, 3, 4$ and $n_F(E_{km}) = 1/(e^{E_{km}/k_B T} + 1)$ is Fermi distribution function with T representing the tem-

perature. Then the order parameter operators are expressed as

$$\begin{aligned}
\delta_{t(b)} &= 1 - \frac{1}{N} \sum_k \sum_{m=1,2,3,4} \left[\xi_{1(2),m}^*(\mathbf{k}) \xi_{1(2),m}(\mathbf{k}) n_F(E_{km}) + \xi_{3(4),m}^*(\mathbf{k}) \xi_{3(4),m}(\mathbf{k}) (1 - n_F(E_{km})) \right], \\
\langle \chi_{t(b)} \rangle &= \frac{1}{N} \sum_k \frac{\cos(k_x) + \cos(k_y)}{2} \sum_{m=1,2,3,4} \left[\xi_{1(2),m}^*(\mathbf{k}) \xi_{1(2),m}(\mathbf{k}) n_F(E_{km}) + \xi_{3(4),m}^*(\mathbf{k}) \xi_{3(4),m}(\mathbf{k}) (1 - n_F(E_{km})) \right], \\
\langle \chi^\perp \rangle &= \frac{1}{N} \sum_k \sum_{m=1,2,3,4} \left[\xi_{1,m}^*(\mathbf{k}) \xi_{2,m}(\mathbf{k}) n_F(E_{km}) + \xi_{4,m}^*(\mathbf{k}) \xi_{3,m}(\mathbf{k}) (1 - n_F(E_{km})) \right], \\
\langle \Delta_{t(b)}^{\mathbf{x}/\mathbf{y}} \rangle^* &= \frac{1}{N} \sum_k 2 \cos(k_{x/y}) \sum_{m=1,2,3,4} \xi_{1(2),m}^*(\mathbf{k}) \xi_{3(4),m}(\mathbf{k}) n_F(E_{km}), \\
\langle \Delta^\perp \rangle &= \frac{2}{N} \sum_k \sum_{m=1,2,3,4} \xi_{1,m}^*(\mathbf{k}) \xi_{4,m}(\mathbf{k}) n_F(E_{km}),
\end{aligned} \tag{S16}$$

where $\xi_{a,m}$ represents the matrix element of ξ at the a -th row and the m -th column.

By solving Eq. (S16) at zero temperature, we obtain the zero-temperature spinon pairing gap. From Eq. (S16), we can also determine the spinon-pairing temperature T_{pair} by solving for the critical condition $\Delta = 0$ at finite temperature. The self-consistent equations are solved by iteration, which is equivalent to finding the minimum value of energy. When solving the self-consistent equations, we assume the pairing symmetry and obtain the energy of the corresponding state. Then the pairing symmetry is determined by the pairing state with the lowest energy. Here we show the energy per site of the s -wave pairing state and the d -wave pairing state relative to the non-superconducting normal state, $(E_s - E_n)/N$ and $(E_d - E_n)/N$, and their difference $(E_s/N) - (E_d/N)$ as functions of the bottom layer $d_{x^2-y^2}$ particle number n_{bx} (Fig. A2). We also consider the $s + id$ -wave pairing, whose expression is actually $\alpha s + i\beta d$, where α and β are variational parameters determined by energy minimization. When one of α and β is zero, the mixed state decays to the s - or d - wave state. For most n_{bx} , we find that one of α and β is zero.

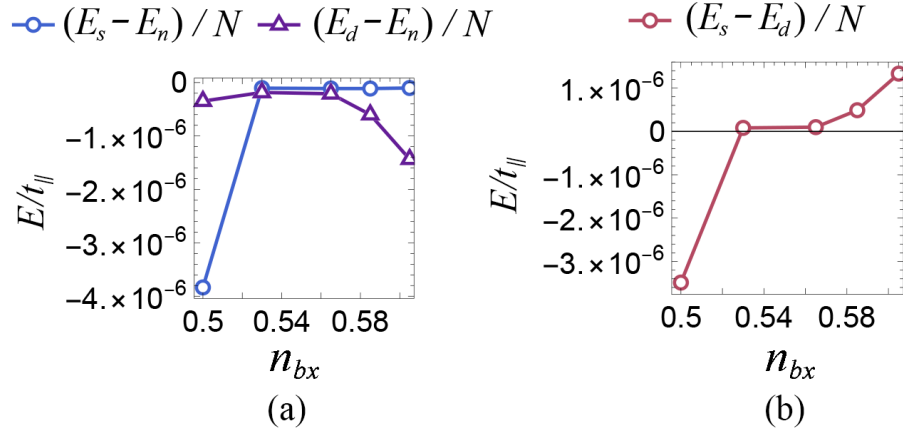


FIG. A2. (a) Energy of the s -wave pairing state relative to that of the non-superconducting normal state $(E_s - E_n)/N$ and that of the d -wave pairing state relative to that of the normal state $(E_d - E_n)/N$, and (b) their difference $(E_s/N) - (E_d/N)$ as functions of the bottom layer $d_{x^2-y^2}$ particle number n_{bx} obtained by the SBMF study for the one orbital model.

To characterize the pairing type of the system, the pairing gap amplitude $\tilde{\Delta}$ is defined as the maximal value of the pairing gaps. For the interlayer s -wave pairing, $\tilde{\Delta} = -\frac{3}{8} \tilde{J}_\perp \langle \Delta^\perp \rangle$. For the d -wave pairing, $\tilde{\Delta} = -\frac{3}{2} J_\parallel \langle \Delta_b^\mathbf{x} \rangle$.

The holon condensation temperature can be calculated according to the Berezinskii-Kosterlitz-Thouless (BKT) transition theory. The holon operator can be written as $b_{i\mu}^\dagger = \sqrt{\delta_\mu} e^{i\theta_\mu(i)}$, whose phase fluctuations lead to the BKT transition. Then the holon Hamiltonian can be written as a XY -model-like form

$$H_{\text{holon}} = -2t_{\parallel} \sum_{\langle i,j \rangle, \mu} \langle \chi_\mu \rangle \delta_\mu \cos(\theta_\mu(i) - \theta_\mu(j)). \tag{S17}$$

We transform the model to a continuous model

$$H_{\text{holon}} \sim \frac{1}{2} \rho \int d^2\mathbf{r} |\nabla\theta|^2, \quad (\text{S18})$$

where

$$\rho = \sum_{|\mu|=1} \sum_{\mu} t_{\parallel} \langle \chi_{\mu} \rangle \delta_{\mu} t^2 \quad (\text{S19})$$

is the superfluid stiffness. Then we can get T_{BEC} from the relationship $T_{\text{BEC}} = (\pi/2)\rho$.

Considering that the real η_1/δ may be different from the TB results, we also study the $\eta_1/\delta = 0/1$ and $\eta_1/\delta = -1/2$ situations (i.e. $(n_{tx} - 0.5)/(n_{bx} - 0.5) = 0/1$ and $(n_{tx} - 0.5)/(n_{bx} - 0.5) = 1/2$). We find that the results of different $(n_{tx} - 0.5)/(n_{bx} - 0.5)$ are similar to each other (shown in Fig. A3 (a)-(c)). Additionally, the d -wave pairing gap $\tilde{\Delta}^d$ is only determined by the particle number n_{bx} but is not related to the particle number ratio $(n_{tx} - 0.5)/(n_{bx} - 0.5)$ (shown in Fig. A3 (d)).

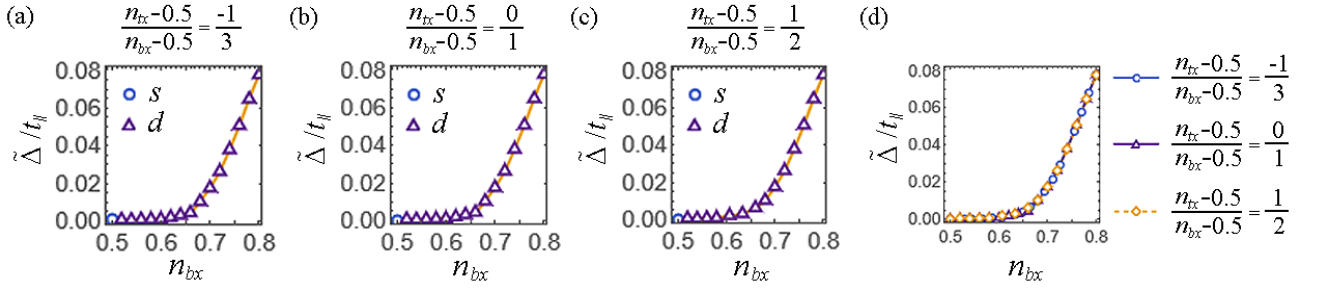


FIG. A3. (a)-(c) The pairing amplitude $\tilde{\Delta}$ (in unit of t_{\parallel}) as function of the bottom-layer particle number n_{bx} controlled by the imposed electric field. Different pairing symmetry is marked by different colors. (d) The pairing gap $\tilde{\Delta}$ of different particle number ratios as function of particle number n_{bx} (represented by different lines). The lines almost coincide with each other especially at the d -wave pairing regime, indicating that the d -wave pairing gap is only determined by the particle number n_{bx} .

We also study how different J_{\perp} affects the result. The relationship between the pairing gap and n_{bx} is calculated when $J_{\perp} = 1.8J_{\parallel}$ as well. The results are shown in Fig. A4. The results of different J_{\perp} are similar to each other and they almost coincide with each other especially at the d -wave pairing regime when plotted together. This indicates that the d -wave pairing gap is not related to J_{\perp} , neither.

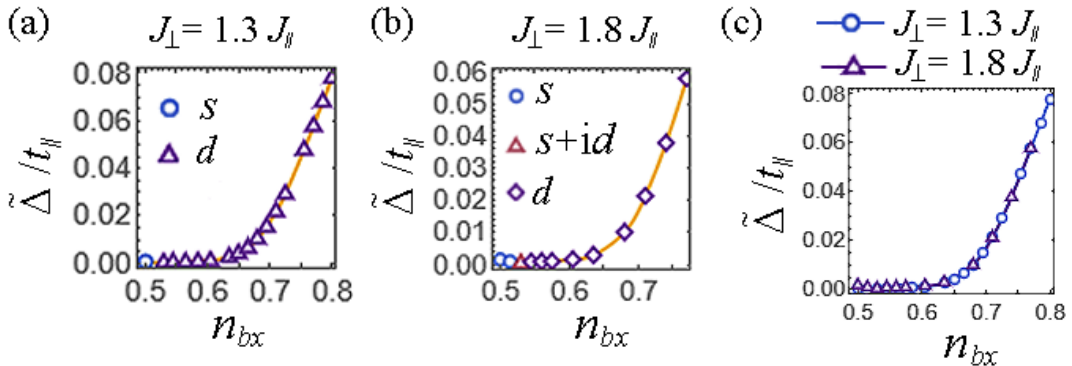


FIG. A4. (a)-(b) The pairing amplitude $\tilde{\Delta}$ (in unit of t_{\parallel}) as function of the bottom-layer particle number n_{bx} controlled by the imposed electric field. Different pairing symmetry is marked by different colors. (c) The pairing gap $\tilde{\Delta}$ of J_{\perp} as function of particle number n_{bx} (represented by different lines). The lines almost coincide with each other especially at the d -wave pairing regime, indicating that the d -wave pairing gap is only determined by the particle number n_{bx} .

B. SLAVE-BOSON MEAN-FIELD TREATMENT OF THE TWO-ORBITAL MODEL

In the two-orbital model, the Hamiltonian takes the form

$$\begin{aligned}
H = & -t_{\parallel} \sum_{\langle i,j \rangle, \mu} \hat{P} \left(c_{i\mu x\sigma}^{\dagger} c_{j\mu x\sigma} + \text{h.c.} \right) \hat{P} - t_{\perp} \sum_i \hat{P} \left(c_{itz\sigma}^{\dagger} c_{ibz\sigma} + \text{h.c.} \right) \hat{P} - t_{xz} \sum_{\langle i,j \rangle, \mu} \hat{P} \left(c_{i\mu x\sigma}^{\dagger} c_{j\mu z\sigma} + (z \leftrightarrow x) + \text{h.c.} \right) \hat{P} \\
& + J_{\parallel} \sum_{\langle i,j \rangle, \mu} \mathbf{S}_{i\mu x} \cdot \mathbf{S}_{j\mu x} + J_{\perp} \sum_i \mathbf{S}_{itz} \cdot \mathbf{S}_{ibz} + \tilde{J}_{\perp} \sum_i \mathbf{S}_{itx} \cdot \mathbf{S}_{ibx} + \epsilon_z \sum_{i\mu\sigma} n_{i\mu z\sigma} + \epsilon_x \sum_{i\mu\sigma} n_{i\mu x\sigma} \\
& + \frac{\varepsilon}{2} \sum_{i\alpha\sigma} n_{it\alpha\sigma} - \frac{\varepsilon}{2} \sum_{i\alpha\sigma} n_{ib\alpha\sigma},
\end{aligned} \tag{S20}$$

where $c_{i\mu z\sigma}^{\dagger}/c_{i\mu x\sigma}^{\dagger}$ creates a $d_{z^2}/d_{x^2-y^2}$ -orbital electron with the spin $\sigma = \{\uparrow, \downarrow\}$ at the lattice site i in the layer $\mu = \{t, b\}$. $n_{i\mu\alpha\sigma} = c_{i\mu\alpha\sigma}^{\dagger} c_{i\mu\alpha\sigma}$ is the particle number operator for the two E_g orbitals with $\alpha = \{z, x\}$. $\mathbf{S}_{i\mu x} = \frac{1}{2} c_{i\mu x\sigma}^{\dagger} [\sigma]_{\sigma\sigma'} c_{i\mu x\sigma'}$ is the spin operator with Pauli matrix $\sigma = (\sigma_x, \sigma_y, \sigma_z)$. ϵ_z and ϵ_x represent the on-site energies of the d_{z^2} and $d_{x^2-y^2}$ orbitals respectively. \hat{P} is a projection operator projecting out the double occupancy in the same orbital of all sites.

We adopt the TB parameters reported in Ref. [141], i.e. $t_{\parallel} = 0.445$ eV, $t_{xz} = 0.221$ eV, $t_{\perp} = 0.503$ eV and $\epsilon_x - \epsilon_z = 0.367$ eV. The spin couplings are estimated as $J_{\parallel(\perp)} = \frac{4t_{\parallel(\perp)}^2}{U}$ with $U = 10t_{\parallel}$ and $\tilde{J}_{\perp} = 0.5J_{\perp}$. To limit the particle numbers of the two E_g orbitals, we consider the Hamiltonian with Lagrange multipliers

$$\tilde{H} = H + (\epsilon'_z - \epsilon_z) \sum_{i\mu\sigma} n_{i\mu z\sigma} + (\epsilon'_x - \epsilon_x) \sum_{i\mu\sigma} n_{i\mu x\sigma}, \tag{S21}$$

where ϵ'_z and ϵ'_x are determined by $n_{bz} = 1$ and $\sum_{\mu\alpha} n_{\mu\alpha} = 3$.

The two-orbital model (S21) is also solved by SBMF theory. The electron operator is decomposed as $c_{i\mu\alpha\sigma}^{\dagger} = f_{i\mu\alpha\sigma}^{\dagger} b_{i\mu\alpha}$, where f is spinon operator and b is holon operator. Since we have found that $T_{\text{BEC}} \gg T_{\text{pair}}$ in the considered n_{bx} regime and T_{pair} is proportional to the zero-temperature spinon pairing gap, we can get the critical temperature of superconductivity only by calculating the ground-state spinon pairing gap. Thus we only consider the spinon Hamiltonian at zero temperature. The superexchange term is also decomposed in $\chi - \Delta$ channel. The spinon Hamiltonian is described as

$$\begin{aligned}
H_{\text{spinon}} = & -t_{\parallel} \sum_{\langle i,j \rangle, \mu} \delta_{\mu x} \left(f_{i\mu x\sigma}^{\dagger} f_{j\mu x\sigma} + \text{h.c.} \right) - t_{xz} \sqrt{\delta_{tx} \delta_{tz}} \sum_{\langle i,j \rangle} \left(f_{itz\sigma}^{\dagger} f_{jtz\sigma} + f_{itz\sigma}^{\dagger} f_{jtx\sigma} + \text{h.c.} \right) \\
& - \frac{3}{8} J_{\parallel} \sum_{\langle i,j \rangle, \mu} \left(\chi_{ij, \mu x}^{\dagger} \langle \chi_{\mu x} \rangle + \text{h.c.} + \Delta_{ij, \mu x}^{\dagger} \langle \Delta_{\mu x} \rangle + \text{h.c.} - \langle \chi_{\mu x}^{\dagger} \rangle \langle \chi_{\mu x} \rangle - \langle \Delta_{\mu x}^{\dagger} \rangle \langle \Delta_{\mu x} \rangle \right) \\
& - \frac{3}{8} J_{\perp} \sum_i \left(\chi_{iz}^{\dagger} \langle \chi_z^{\perp} \rangle + \text{h.c.} + \Delta_{iz}^{\dagger} \langle \Delta_z^{\perp} \rangle + \text{h.c.} - \langle \chi_z^{\perp} \rangle \langle \chi_z^{\perp} \rangle - \langle \Delta_z^{\perp} \rangle \langle \Delta_z^{\perp} \rangle \right) \\
& - \frac{3}{8} \tilde{J}_{\perp} \sum_i \left(\Delta_{ix}^{\dagger} \langle \Delta_x^{\perp} \rangle + \text{h.c.} - \langle \Delta_x^{\perp} \rangle \langle \Delta_x^{\perp} \rangle \right) \\
& + \epsilon'_z \sum_{i\mu\sigma} n_{i\mu z\sigma} + \epsilon'_x \sum_{i\mu\sigma} n_{i\mu x\sigma} + \frac{\varepsilon}{2} \sum_{i\alpha\sigma} n_{it\alpha\sigma} - \frac{\varepsilon}{2} \sum_{i\alpha\sigma} n_{ib\alpha\sigma},
\end{aligned} \tag{S22}$$

where $\delta_{\mu\alpha} = \langle b_{i\mu\alpha} b_{j\mu\alpha}^{\dagger} \rangle$ since holon condense at zero temperature. Under the electric field, we have $\delta_{bz} = 0$ and δ_{tz} ,

δ_{tx} and δ_{bx} are solved self-consistently. The mean-field order parameters are represented by

$$\begin{aligned}
\chi_{ij,\mu x} &= \sum_{\sigma} f_{i\mu x\sigma}^{\dagger} f_{j\mu x\sigma}, \quad \chi_{\mu x} = \frac{1}{2N} \sum_{\langle i,j \rangle} \chi_{ij,\mu x}, \\
\chi_{iz}^{\perp\dagger} &= \sum_{\sigma} f_{izt\sigma}^{\dagger} f_{izb\sigma}, \quad \chi_z^{\perp} = \frac{1}{N} \sum_i \chi_{iz}^{\perp}, \\
\Delta_{ij,\mu\alpha}^{\dagger} &= f_{i\mu\alpha\uparrow}^{\dagger} f_{j\mu\alpha\downarrow}^{\dagger} - f_{i\mu\alpha\downarrow}^{\dagger} f_{j\mu\alpha\uparrow}^{\dagger}, \quad \Delta_{\mu x}^{\mathbf{x}(\mathbf{y})} = \frac{1}{2N} \sum_{\mathbf{R}_i - \mathbf{R}_j = \pm \mathbf{x}(\mathbf{y})} \Delta_{ij,\mu x}, \\
\Delta_{i\alpha}^{\perp\dagger} &= f_{it\alpha\uparrow}^{\dagger} f_{ib\alpha\downarrow}^{\dagger} - f_{ib\alpha\downarrow}^{\dagger} f_{it\alpha\uparrow}^{\dagger}, \quad \Delta_{\alpha}^{\perp} = \frac{1}{N} \sum_i \Delta_{i\alpha}^{\perp}.
\end{aligned} \tag{S23}$$

Notably, the spin-exchange \tilde{J}_{\perp} of the Hamiltonian in Eq. (S20) doesn't produce a hopping term χ_x^{\perp} in Eq. (S22), which is the feature of such a bilayer system. Without interlayer hopping, a small interlayer spin-exchange J_{\perp} leads to $\langle \chi^{\perp} \rangle \approx 0$.

Consequently, the $3d_{z^2}$ orbital only participate in the interlayer pairing. However, this pairing is not superconductivity (SC) as the corresponding SC order parameter goes to zero in the SBMF theory due to $\delta_{bz} = 0$. The SC is carried by the $3d_{x^2-y^2}$ orbitals, which can form both intralayer and interlayer pairing. The superconducting T_c scales with the ground state gap amplitude of the $3d_{x^2-y^2}$ orbitals via the Bardeen-Cooper-Schrieffer (BCS) relation exhibited in Fig. 3(b) in the main text.

The expectation value of the mean-field order parameters are obtained by numerically solving the following self-consistent equations

$$\begin{aligned}
\delta_{\mu\alpha} &= 1 - \frac{1}{N} \sum_k \left(\langle f_{k\mu\alpha\uparrow}^{\dagger} f_{k\mu\alpha\uparrow} \rangle + \langle f_{-k\mu\alpha\downarrow}^{\dagger} f_{-k\mu\alpha\downarrow} \rangle \right), \quad \delta_{tz} = 0, \quad \sum_{\mu\alpha} \delta_{\mu\alpha} = 1, \\
\langle \chi_{\mu x} \rangle &= \frac{1}{N} \sum_{\langle i,j \rangle} \langle \chi_{ij,\mu x} \rangle = \frac{1}{N} \sum_k \frac{\cos(k_x) + \cos(k_y)}{2} \left(\langle f_{k\mu x\uparrow}^{\dagger} f_{k\mu x\uparrow} \rangle + \langle f_{-k\mu x\downarrow}^{\dagger} f_{-k\mu x\downarrow} \rangle \right), \\
\langle \chi_z^{\perp} \rangle &= \frac{1}{N} \sum_i \langle \chi_{iz}^{\perp} \rangle = \frac{1}{N} \sum_k \left(\langle f_{ktz\uparrow}^{\dagger} f_{kbz\uparrow} \rangle + \langle f_{-ktz\downarrow}^{\dagger} f_{-kbz\downarrow} \rangle \right), \\
\langle \Delta_{\mu x}^{\mathbf{x}(\mathbf{y})} \rangle^* &= \frac{1}{2N} \sum_{\mathbf{R}_i - \mathbf{R}_j = \pm \mathbf{x}(\mathbf{y})} \langle \Delta_{ij,\mu x} \rangle^* = \frac{1}{N} \sum_k 2 \cos(k_x(y)) \langle f_{k\mu x\uparrow}^{\dagger} f_{-k\mu x\downarrow}^{\dagger} \rangle, \\
\langle \Delta_{\alpha}^{\perp} \rangle^* &= \frac{1}{N} \sum_i \langle \Delta_{i\alpha}^{\perp} \rangle^* = \frac{2}{N} \sum_k \langle f_{kt\alpha\uparrow}^{\dagger} f_{-kb\alpha\downarrow}^{\dagger} \rangle.
\end{aligned} \tag{S24}$$

Here, $f_{\mathbf{k}\mu\alpha\sigma} = \frac{1}{\sqrt{N}} \sum_i f_{i\mu\alpha\sigma} e^{-i\mathbf{k}\cdot\mathbf{R}_i}$, $k_{x/y}$ is the x/y -component of \mathbf{k} , and $\langle \Delta_{\mu x}^{\mathbf{x}/\mathbf{y}} \rangle$ is the $d_{x^2-y^2}$ -electron-pairing gap of the nearest neighbor bond along the x/y direction.

In the self consistent equations, the expectation values of the operators are obtained as follows. The matrix form of the spinon Hamiltonian is

$$H_{\text{spinon}} = \sum_k \begin{pmatrix} f_{ktz\uparrow}^{\dagger} & f_{ktx\uparrow}^{\dagger} & f_{kbz\uparrow}^{\dagger} & f_{kbx\uparrow}^{\dagger} & f_{-ktz\downarrow} & f_{-ktx\downarrow} & f_{-kbz\downarrow} & f_{-kbx\downarrow} \end{pmatrix} \begin{pmatrix} H_{\chi}(\mathbf{k}) & H_{\Delta}(\mathbf{k}) \\ H_{\Delta}^{\dagger}(\mathbf{k}) & -H_{\chi}^T(\mathbf{k}) \end{pmatrix} \begin{pmatrix} f_{ktz\uparrow} \\ f_{ktx\uparrow} \\ f_{kbz\downarrow} \\ f_{kbx\downarrow} \\ f_{-ktz\downarrow}^{\dagger} \\ f_{-ktx\downarrow}^{\dagger} \\ f_{-kbz\downarrow}^{\dagger} \\ f_{-kbx\downarrow}^{\dagger} \end{pmatrix}, \tag{S25}$$

where

$$H_\chi(\mathbf{k}) = \begin{pmatrix} h_{11}(\mathbf{k}) & h_{12}(\mathbf{k}) & h_{13}(\mathbf{k}) & h_{14}(\mathbf{k}) \\ h_{21}(\mathbf{k}) & h_{22}(\mathbf{k}) & h_{23}(\mathbf{k}) & h_{24}(\mathbf{k}) \\ h_{31}(\mathbf{k}) & h_{32}(\mathbf{k}) & h_{33}(\mathbf{k}) & h_{34}(\mathbf{k}) \\ h_{41}(\mathbf{k}) & h_{42}(\mathbf{k}) & h_{43}(\mathbf{k}) & h_{44}(\mathbf{k}) \end{pmatrix},$$

$$h_{11}(\mathbf{k}) = \epsilon'_z + \frac{\varepsilon}{2}, \quad h_{33}(\mathbf{k}) = \epsilon'_z - \frac{\varepsilon}{2}, \quad h_{13}(\mathbf{k}) = h_{31}(\mathbf{k}) = -t_\perp \sqrt{\delta_{tz}\delta_{bz}} - \frac{3}{8}J_\perp \langle \chi_z^\perp \rangle,$$

$$h_{22}(\mathbf{k}) = -2 \left(t_\parallel \delta_{tx} + \frac{3}{8}J_\parallel \langle \chi_{tx} \rangle \right) (\cos(k_x) + \cos(k_y)) + \epsilon'_x + \frac{\varepsilon}{2},$$

$$h_{44}(\mathbf{k}) = -2 \left(t_\parallel \delta_{bx} + \frac{3}{8}J_\parallel \langle \chi_{bx} \rangle \right) (\cos(k_x) + \cos(k_y)) + \epsilon'_x - \frac{\varepsilon}{2},$$

$$h_{12}(\mathbf{k}) = h_{21}(\mathbf{k}) = -2t_{xz} \sqrt{\delta_{tz}\delta_{tx}} (\cos(k_x) - \cos(k_y)), \quad h_{34}(\mathbf{k}) = h_{43}(\mathbf{k}) = -2t_{xz} \sqrt{\delta_{bz}\delta_{bx}} (\cos(k_x) - \cos(k_y)),$$

$$h_{14}(\mathbf{k}) = h_{41}(\mathbf{k}) = h_{23}(\mathbf{k}) = h_{32}(\mathbf{k}) = h_{24}(\mathbf{k}) = h_{42}(\mathbf{k}) = 0,$$

$$H_\Delta(\mathbf{k}) = \begin{pmatrix} 0 & 0 & -\frac{3}{8}J_\perp \langle \Delta_z^\perp \rangle & 0 \\ 0 & -\frac{3}{4}J_\parallel (\langle \Delta_{tx}^\mathbf{x} \rangle \cos(k_x) + \langle \Delta_{tx}^\mathbf{y} \rangle \cos(k_y)) & 0 & -\frac{3}{8}\tilde{J}_\perp \langle \Delta_x^\perp \rangle \\ -\frac{3}{8}J_\perp \langle \Delta_z^\perp \rangle & 0 & 0 & 0 \\ 0 & -\frac{3}{8}\tilde{J}_\perp \langle \Delta^\perp \rangle & 0 & -\frac{3}{4}J_\parallel (\langle \Delta_{bx}^\mathbf{x} \rangle \cos(k_x) + \langle \Delta_{bx}^\mathbf{y} \rangle \cos(k_y)) \end{pmatrix}. \quad (\text{S26})$$

H_{spinon} can be diagonalized by a Bogoliubov transformation.

$$H_{\text{spinon}} = \sum_k (\gamma_{k1}^\dagger \cdots \gamma_{k8}^\dagger) \text{diag}(E_{k1}, \dots, E_{k8}) \begin{pmatrix} \gamma_{k1} \\ \vdots \\ \gamma_{k8} \end{pmatrix}, \quad (\text{S27})$$

where

$$\xi^\dagger(\mathbf{k}) \begin{pmatrix} H_\chi(\mathbf{k}) & H_\Delta(\mathbf{k}) \\ H_\Delta^\dagger(\mathbf{k}) & -H_\chi^T(\mathbf{k}) \end{pmatrix} \xi(\mathbf{k}) = \text{diag}(E_{k1}, \dots, E_{k8}), \quad \begin{pmatrix} f_{ktz\uparrow} \\ f_{ktx\uparrow} \\ f_{k bz\uparrow} \\ f_{k bx\uparrow} \\ f_{-ktz\downarrow}^\dagger \\ f_{-ktx\downarrow}^\dagger \\ f_{-k bz\downarrow}^\dagger \\ f_{-k bx\downarrow}^\dagger \end{pmatrix} = \xi(\mathbf{k}) \begin{pmatrix} \gamma_{k1} \\ \vdots \\ \gamma_{k8} \end{pmatrix}. \quad (\text{S28})$$

Here, γ is fermionic operator, whose expectation value is

$$\langle \gamma_{km}^\dagger \gamma_{k'n} \rangle = \delta_{kk'} \delta_{mn} n_F(E_{km}), \quad \langle \gamma_{km} \gamma_{k'n} \rangle = \langle \gamma_{km}^\dagger \gamma_{k'n}^\dagger \rangle = 0, \quad (\text{S29})$$

where $m = 1, \dots, 8$ and $n_F(E_{km}) = 1/(e^{E_{km}/k_B T} + 1)$ is Fermi distribution function with T representing the temperature. Then the order parameter operators are expressed as

$$\begin{aligned} \delta_{tz(tx, bz, bx)} &= 1 - \frac{1}{N} \sum_k \sum_{m=1, \dots, 8} \left[\xi_{1(2,3,4),m}^*(\mathbf{k}) \xi_{1(2,3,4),m}(\mathbf{k}) n_F(E_{km}) + \xi_{5(6,7,8),m}^*(\mathbf{k}) \xi_{5(6,7,8),m}(\mathbf{k}) (1 - n_F(E_{km})) \right], \\ \langle \chi_{tx(bx)} \rangle &= \frac{1}{N} \sum_k \frac{\cos(k_x) + \cos(k_y)}{2} \sum_{m=1, \dots, 8} \left[\xi_{2(4),m}^*(\mathbf{k}) \xi_{2(4),m}(\mathbf{k}) n_F(E_{km}) + \xi_{6(8),m}^*(\mathbf{k}) \xi_{6(8),m}(\mathbf{k}) (1 - n_F(E_{km})) \right], \\ \langle \chi_z^\perp \rangle &= \frac{1}{N} \sum_k \sum_{m=1, \dots, 8} \left[\xi_{1,m}^*(\mathbf{k}) \xi_{3,m}(\mathbf{k}) n_F(E_{km}) + \xi_{7,m}^*(\mathbf{k}) \xi_{5,m}(\mathbf{k}) (1 - n_F(E_{km})) \right], \\ \langle \Delta_{tx(bx)}^{\mathbf{x}/\mathbf{y}} \rangle^* &= \frac{1}{N} \sum_k 2 \cos(k_{x/y}) \sum_{m=1, \dots, 8} \xi_{2(4),m}^*(\mathbf{k}) \xi_{6(8),m}(\mathbf{k}) n_F(E_{km}), \\ \langle \Delta_{z(x)}^\perp \rangle &= \frac{2}{N} \sum_k \sum_{m=1, \dots, 8} \xi_{1(2),m}^*(\mathbf{k}) \xi_{7(8),m}(\mathbf{k}) n_F(E_{km}), \end{aligned} \quad (\text{S30})$$

where $\xi_{a,m}$ represents the matrix element of ξ at the a -th row and the m -th column. The method to solve these self-consistent equations is similar to the one to solve the one-orbital model.

In the two-orbital model, the pairing gap amplitude $\tilde{\Delta}_x$ is defined as the maximal value of the pairing gap of the $3d_{x^2-y^2}$ electrons. For the interlayer s -wave pairing, $\tilde{\Delta}_x = -\frac{3}{8}\tilde{J}_\perp \langle \Delta_x^\perp \rangle$. For the $(s(d_{z^2})+id(d_{x^2-y^2}))$ -wave pairing, $\tilde{\Delta}_x = -\frac{3}{2}J_\parallel \langle \Delta_{bx}^\times \rangle$.

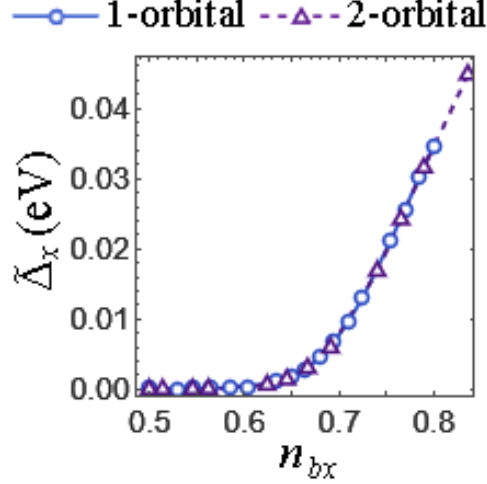


FIG. A5. The comparison of the pairing amplitude $\tilde{\Delta}_x$ as function of the bottom-layer particle number n_{bx} calculated with different models. The lines almost coincide with each other, particularly in the large- n_{bx} regime.

We find that the pairing amplitude $\tilde{\Delta}_x$ as function of the bottom-layer particle number n_{bx} calculated with different models show a strong resemblance (see Fig. A5).

C. MORE NUMERICAL SIMULATION RESULTS BY DENSITY MATRIX RENORMALIZATION GROUP

We apply the density matrix renormalization group (DMRG) approach [158, 159] to solve the ground state of Hamiltonian (S1) with $t_\parallel = 1$, $J_\parallel = 0.4t_\parallel$ and $\tilde{J}_\perp = 0.8J_\parallel$. The definitions of all the operators and main results have been shown in the main text. Here we give more results.

In Fig. A6, we show the absolute value of correlation functions $|\Phi^\perp(r)|$ and $|\Phi_t^{\times y}(r)|$ for comparison with Fig. 4 in the main text. It turns out that the external electric field suppresses interlayer pairing across different electron-doped levels, while it notably strengthens intra-bottom-layer pairing by increasing carrier concentration.

Fig. A7 shows the particle number distribution in the two layers for different (δ, ε) . As shown in Fig. A7 (a) and (c), the expectation of electron number in the two layers is equal without an external electric field. Fig. A7 (b) and (d) exhibit that when a perpendicular electric field is introduced, electrons flow from the top layer with a lower electric potential to the bottom layer with a higher electric potential.

We also consider the single particle Green's function, defined as

$$G_\mu(r) = \sum_\sigma \langle c_{i\mu\sigma}^\dagger c_{j\mu\sigma} \rangle \quad (\mu = t, b). \quad (\text{S31})$$

The results are shown in Fig. A8. The Green's function under all of the parameters exhibits exponential decay.

D. THE EFFECT OF INTERLAYER COULOMB INTERACTION

In order to better capture the properties of $\text{La}_3\text{Ni}_2\text{O}_7$ thin films, we further consider the effect of interlayer Coulomb interaction in the single-orbital model and solve it using both SBMF and DMRG methods, respectively. The modified

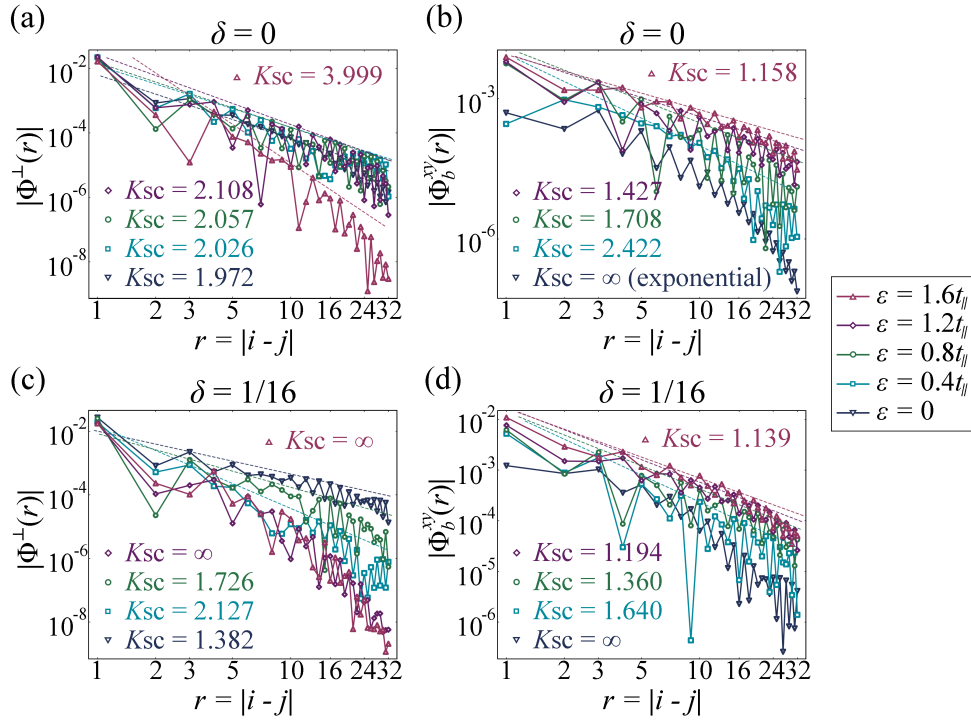


FIG. A6. (a)-(d) The interlayer pairing correlation functions $|\Phi^{\perp}(r)|$ and intralayer correlation functions $|\Phi_b^{xy}(r)|$ under different electronic field $\varepsilon = 0, 0.4t_{\parallel}, 0.8t_{\parallel}, 1.2t_{\parallel}, 1.6t_{\parallel}$ for $\delta = 0$ in (a)-(b) and $\delta = 1/16$ in (c)-(d). The decay exponents K_{sc} are written in the figures as well.

Hamiltonian is

$$H = -t_{\parallel} \sum_{\langle i,j \rangle, \mu, \sigma} \hat{P} \left(c_{i\mu\sigma}^{\dagger} c_{j\mu\sigma} + \text{h.c.} \right) \hat{P} + \sum_{i, \mu} \epsilon_{\mu} n_{i\mu} + J_{\parallel} \sum_{\langle i,j \rangle, \mu} \mathbf{S}_{i\mu} \cdot \mathbf{S}_{j\mu} + \tilde{J}_{\perp} \sum_i \mathbf{S}_{it} \cdot \mathbf{S}_{ib} + V \sum_i n_{it} n_{ib}, \quad (\text{S32})$$

where V is the strength of the interlayer Coulomb interaction.

In the SBMF method, the additional terms are decomposed as

$$\begin{aligned} V \sum_i n_{it} n_{ib} &\rightarrow V \sum_i (\langle n_t \rangle n_{ib} + \langle n_b \rangle n_{it} - \langle n_t \rangle \langle n_b \rangle) \\ &\quad - \frac{1}{2} V \sum_i \left(\chi_{iz}^{\perp\dagger} \langle \chi_z^{\perp} \rangle + \text{h.c.} - \langle \chi_z^{\perp\dagger} \rangle \langle \chi_z^{\perp} \rangle \right) \\ &\quad + \frac{1}{2} V \sum_i \left(\Delta_{iz}^{\perp\dagger} \langle \Delta_z^{\perp} \rangle + \text{h.c.} - \langle \Delta_z^{\perp\dagger} \rangle \langle \Delta_z^{\perp} \rangle \right), \end{aligned} \quad (\text{S33})$$

where $\langle n_{\mu} \rangle = n_{\mu}$ is average particle number expectation for layer $\mu = t, b$. The expectation value of the first term is

$$VN \langle n_t \rangle \langle n_b \rangle = \frac{VN}{4} (\langle n_t \rangle + \langle n_b \rangle)^2 - \frac{VN}{4} (\langle n_b \rangle - \langle n_t \rangle)^2, \quad (\text{S34})$$

indicating that the V term favors the difference of the particle number of different layers by lower the energy. The expectation value of the last term is

$$+ \frac{VN}{2} |\langle \Delta^{\perp} \rangle|^2, \quad (\text{S35})$$

therefore the V term is expected to suppress the interlayer pairing by lifting its energy.

Fig. A9 shows the SBMF results, exhibiting the relationship between external electric field ε and the interlayer Coulomb interaction V with the same particle number distribution and the same d -wave pairing gap. The results

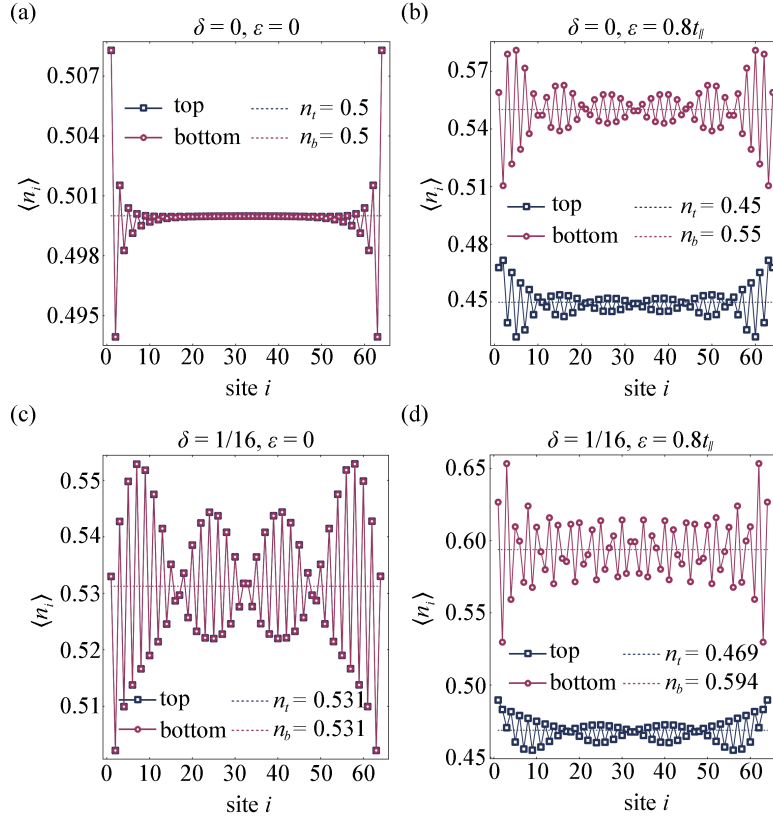


FIG. A7. (a)-(d) The particle number distribution in the two layers for different parameters $(\delta, \varepsilon) = (0, 0)$, $(0, 0.8t_{\parallel})$, $(1/16, 0)$ and $(1/16, 0.8t_{\parallel})$. The dashed lines correspond to the total expectation of the number of electrons in each of the two layers.

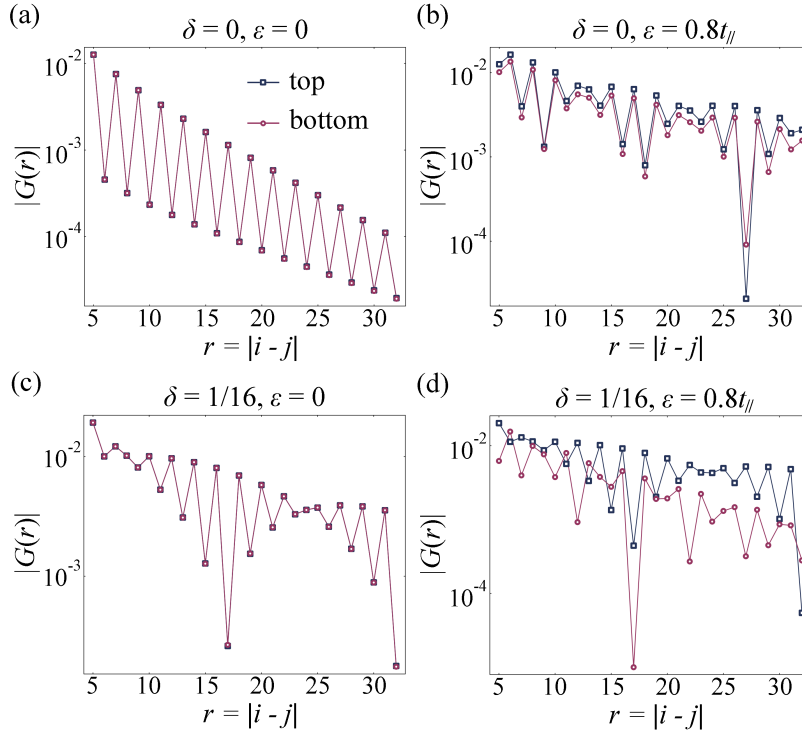


FIG. A8. (a)-(d) The single particle Green's function $|G(r)|$ for $(\delta, \varepsilon) = (0, 0)$, $(0, 0.8t_{\parallel})$, $(1/16, 0)$ and $(1/16, 0.8t_{\parallel})$.

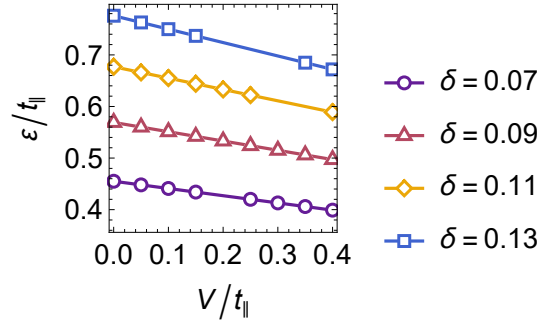


FIG. A9. The relationship between external electric field ε and interlayer Coulomb interaction V for realizing the same particle number distribution ($n_t = 0.5 - \delta/2$ and $n_b = 0.5 + 3\delta/2$) and the same d -wave pairing gap (obtained by SBMF approach).

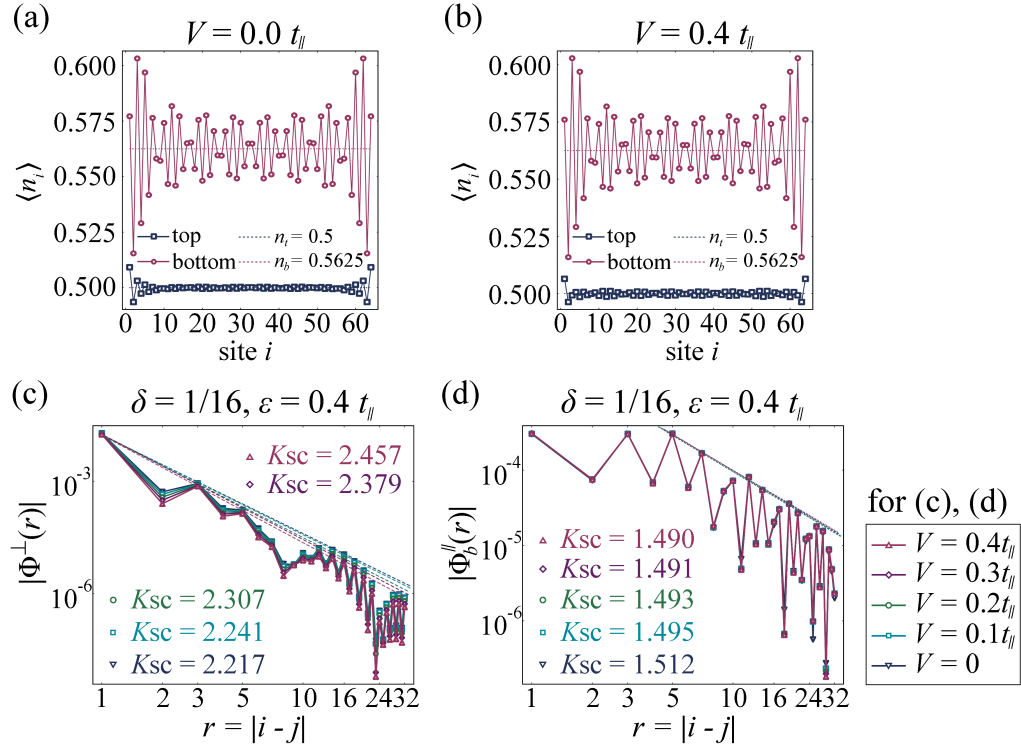


FIG. A10. DMRG results for the Hamiltonian Eq. (S32) including the interlayer Coulomb interaction V -term. (a) The interlayer pairing correlation functions $|\Phi^\pm(r)|$ for different V within $V = 0 \sim 0.4t_{||}$. (b) The intra-bottom-layer pairing correlation functions $|\Phi_b^\parallel(r)|$ for different V within $V = 0 \sim 0.4t_{||}$. The algebraic decay coefficient K_{sc} reflects the decay rate of the pairing correlation function with spatial distance, negatively correlated with the corresponding pairing strength.

display that, when realizing the same particle number distribution ($n_t = 0.5 - \delta/2$ and $n_b = 0.5 + 3\delta/2$) and the same pairing gap, the external electric field ε slightly decreases as the interlayer Coulomb interaction V increases, indicating that interlayer Coulomb interaction slightly promotes charge transfer between layers. Therefore, if the external electric field ε is fixed, introducing interlayer Coulomb interaction will slightly increase the difference of the particle number of the two layers as well as the particle number of the bottom layer, and thus will increase the critical temperature of d -wave pairing, which only depends on the particle number of the bottom layer.

The DMRG results shown in Fig. A10 illustrates the trend of the properties of ground state with different interlayer Coulomb interactions $V = 0 \sim 0.4t_{||}$. Here we take the transferred $d_{x^2-y^2}$ -electron-doping level $\delta = 1/16$ and $\varepsilon = 0.4t_{||}$ for a typical analysis, and the other parameters are consistent with the main text. Fig. A10 (a) and (b) show the particle number distributions for $V = 0$ and $0.4t_{||}$, and the results indicate that the interlayer Coulomb interaction does not have an observable effect on the particle number distributions, which may also be affected by the finite size.

Fig. A10 (c) and (d) exhibit the trends of interlayer superconducting pairing and intralayer pairing with different V , respectively. According to the trend of the algebraic decay coefficient K_{SC} shown in Fig. A10, the interlayer pairing is suppressed with the enhancement of V , while the intra-bottom-layer pairing demonstrates slight enhancement, which is qualitatively consistent with the SBMF results.

In conclusion, the combined SBMF and DMRG results show that the introduction of interlayer Coulomb interaction slightly increases the particle number difference between the two layers and the strength of intra-bottom-layer pairing, while suppressing interlayer pairing.

-
- * These two authors contributed equally to this work.
† yangfan_blg@bit.edu.cn
- [1] H. Sun, M. Huo, X. Hu, J. Li, Z. Liu, Y. Han, L. Tang, Z. Mao, P. Yang, B. Wang, J. Cheng, D.-X. Yao, G.-M. Zhang, and M. Wang, Signatures of superconductivity near 80K in a nickelate under high pressure, *Nature* **621**, 493 (2023).
 - [2] Y. Zhang, D. Su, Y. Huang, Z. Shan, H. Sun, M. Huo, K. Ye, J. Zhang, Z. Yang, Y. Xu, Y. Su, R. Li, M. Smidman, M. Wang, L. Jiao, and H. Yuan, High-temperature superconductivity with zero resistance and strange-metal behaviour in $\text{La}_3\text{Ni}_2\text{O}_{7-\delta}$, *Nat. Phys.* **20**, 1269 (2024).
 - [3] J. Hou, P.-T. Yang, Z.-Y. Liu, J.-Y. Li, P.-F. Shan, L. Ma, G. Wang, N.-N. Wang, H.-Z. Guo, J.-P. Sun, Y. Uwatoko, M. Wang, G.-M. Zhang, B.-S. Wang, and J.-G. Cheng, Emergence of high-temperature superconducting phase in pressurized $\text{La}_3\text{Ni}_2\text{O}_7$ crystals, *Chin. Phys. Lett.* **40**, 117302 (2023).
 - [4] G. Wang, N. N. Wang, X. L. Shen, J. Hou, L. Ma, L. F. Shi, Z. A. Ren, Y. D. Gu, H. M. Ma, P. T. Yang, Z. Y. Liu, H. Z. Guo, J. P. Sun, G. M. Zhang, S. Calder, J.-Q. Yan, B. S. Wang, Y. Uwatoko, and J.-G. Cheng, Pressure-induced superconductivity in polycrystalline $\text{La}_3\text{Ni}_2\text{O}_7$, *Phys. Rev. X* **14**, 011040 (2024).
 - [5] G. Wang, N. Wang, Y. Wang, L. Shi, X. Shen, J. Hou, H. Ma, P. Yang, Z. Liu, H. Zhang, X. Dong, J. Sun, B. Wang, K. Jiang, J. Hu, Y. Uwatoko, and J. Cheng, Observation of high-temperature superconductivity in the high-pressure tetragonal phase of $\text{La}_2\text{PrNi}_2\text{O}_{7-\delta}$, [arXiv:2311.08212](https://arxiv.org/abs/2311.08212) (2023).
 - [6] M. Zhang, C. Pei, Q. Wang, Y. Zhao, C. Li, W. Cao, S. Zhu, J. Wu, and Y. Qi, Effects of pressure and doping on Ruddlesden-Popper phases $\text{La}_{n+1}\text{Ni}_n\text{O}_{3n+1}$, *J. Mater. Sci. Technol.* **185**, 147 (2024).
 - [7] Y. Zhou, J. Guo, S. Cai, H. Sun, C. Li, J. Zhao, P. Wang, J. Han, X. Chen, Y. Chen, Q. Wu, Y. Ding, T. Xiang, H.-k. Mao, and L. Sun, Investigations of key issues on the reproducibility of high- T_c superconductivity emerging from compressed $\text{La}_3\text{Ni}_2\text{O}_7$, *Matter and Radiation at Extremes* **10** (2025).
 - [8] N. Wang, G. Wang, X. Shen, J. Hou, J. Luo, X. Ma, H. Yang, L. Shi, J. Dou, J. Feng, J. Yang, Y. Shi, Z. Ren, H. Ma, P. Yang, Z. Liu, Y. Liu, H. Zhang, X. Dong, Y. Wang, K. Jiang, J. Hu, S. Calder, J. Yan, J. Sun, B. Wang, R. Zhou, Y. Uwatoko, and J. Cheng, Bulk high-temperature superconductivity in the high-pressure tetragonal phase of bilayer $\text{La}_2\text{PrNi}_2\text{O}_7$, *Nature* **634**, 579 (2024).
 - [9] J. Li, D. Peng, P. Ma, H. Zhang, Z. Xing, X. Huang, C. Huang, M. Huo, D. Hu, Z. Dong, X. Chen, T. Xie, H. Dong, H. Sun, Q. Zeng, H.-k. Mao, and M. Wang, Identification of the superconductivity in bilayer nickelate $\text{La}_3\text{Ni}_2\text{O}_7$ upon 100 gpa, [arXiv:2404.11369](https://arxiv.org/abs/2404.11369) (2024).
 - [10] T. Fukamachi, Y. Kobayashi, T. Miyashita, and M. Sato, ^{139}La NMR studies of layered perovskite systems $\text{La}_3\text{Ni}_2\text{O}_{7-\delta}$ and $\text{La}_4\text{Ni}_3\text{O}_{10}$, *J. Phys. Chem. Solids* **62**, 195 (2001).
 - [11] R. Khasanov, T. J. Hicken, D. J. Gawryluk, V. Sazgari, I. Plokhikh, L. P. Sorel, M. Bartkowiak, S. Bötzel, F. Lechermann, I. M. Eremin, H. Luetkens, and Z. Guguchia, Pressure-enhanced splitting of density wave transitions in $\text{La}_3\text{Ni}_2\text{O}_{7-\delta}$, *Nature Physics* **21**, 430 (2025).
 - [12] K. Chen, X. Liu, J. Jiao, M. Zou, C. Jiang, X. Li, Y. Luo, Q. Wu, N. Zhang, Y. Guo, and L. Shu, Evidence of spin density waves in $\text{La}_3\text{Ni}_2\text{O}_{7-\delta}$, *Phys. Rev. Lett.* **132**, 256503 (2024).
 - [13] D. Zhao, Y. Zhou, M. Huo, Y. Wang, L. Nie, Y. Yang, J. Ying, M. Wang, T. Wu, and X. Chen, Pressure-enhanced spin-density-wave transition in double-layer nickelate $\text{La}_3\text{Ni}_2\text{O}_{7-\delta}$, *Science Bulletin* **70**, 1239 (2025).
 - [14] X. Chen, J. Choi, Z. Jiang, J. Mei, K. Jiang, J. Li, S. Agrestini, M. Garcia-Fernandez, X. Huang, H. Sun, D. Shen, M. Wang, J. Hu, Y. Lu, K.-J. Zhou, and D. Feng, Electronic and magnetic excitations in $\text{La}_3\text{Ni}_2\text{O}_7$, *Nature Communications* **15**, 9597 (2024).
 - [15] Z. Liu, H. Sun, M. Huo, X. Ma, Y. Ji, E. Yi, L. Li, H. Liu, J. Yu, Z. Zhang, Z. Chen, F. Liang, H. Dong, H. Guo, D. Zhong, B. Shen, S. Li, and M. Wang, Evidence for charge and spin density waves in single crystals of $\text{La}_3\text{Ni}_2\text{O}_7$ and $\text{La}_3\text{Ni}_2\text{O}_{6,\delta}$, *Sci. China-Phys. Mech. Astron.* **66**, 217411 (2023).
 - [16] M. Kakoi, T. Oi, Y. Ohshita, M. Yashima, K. Kuroki, T. Kato, H. Takahashi, S. Ishiwata, Y. Adachi, N. Hatada, T. Uda, and H. Mukuda, Multiband metallic ground state in multilayered nickelates $\text{La}_3\text{Ni}_2\text{O}_7$ and $\text{La}_4\text{Ni}_3\text{O}_{10}$ probed by ^{139}La -NMR at ambient pressure, *J. Phys. Soc. Jpn.* **93**, 053702 (2024).
 - [17] T. Xie, M. Huo, X. Ni, F. Shen, X. Huang, H. Sun, H. C. Walker, D. Adroja, D. Yu, B. Shen, L. He, K. Cao, and M. Wang, Strong interlayer magnetic exchange coupling in $\text{La}_3\text{Ni}_2\text{O}_{7-\delta}$ revealed by inelastic neutron scattering, *Sci. Bull.* **69**, 3221 (2024).
 - [18] N. K. Gupta, R. Gong, Y. Wu, M. Kang, C. T. Parzyck, B. Z. Gregory, N. Costa, R. Sutarto, S. Sarker, A. Singer, D. G. Schlom, K. M. Shen, and D. G. Hawthorn, Anisotropic spin stripe domains in bilayer $\text{La}_3\text{Ni}_2\text{O}_7$, [arXiv:2409.03210](https://arxiv.org/abs/2409.03210) (2024).
 - [19] X. Ren, R. Sutarto, X. Wu, J. Zhang, H. Huang, T. Xiang, J. Hu, R. Comin, X. Zhou, and Z. Zhu, Resolving the electronic ground state of $\text{La}_3\text{Ni}_2\text{O}_{7-\delta}$ films, *Communications Physics* **8**, 52 (2025).
 - [20] J.-J. Feng, T. Han, J.-P. Song, M.-S. Long, X.-Y. Hou, C.-J. Zhang, Q.-G. Mu, and L. Shan, Unaltered density wave transition and pressure-induced signature of superconductivity in Nd-doped $\text{La}_3\text{Ni}_2\text{O}_7$, *Phys. Rev. B* **110**, L100507 (2024).
 - [21] Y. Meng, Y. Yang, H. Sun, S. Zhang, J. Luo, L. Chen, X. Ma, M. Wang, F. Hong, X. Wang, and X. Yu, Density-wave-like gap evolution in $\text{La}_3\text{Ni}_2\text{O}_7$ under high pressure revealed by ultrafast optical spectroscopy, *Nature Communications* **15**, 10408 (2024).
 - [22] S. Fan, Z. Luo, M. Huo, Z. Wang, H. Li, H. Yang, M. Wang, D.-X. Yao, and H.-H. Wen, Tunneling spectra with gaplike features observed in nickelate $\text{La}_3\text{Ni}_2\text{O}_7$ at ambient pressure, *Phys. Rev. B* **110**, 134520 (2024).
 - [23] M. Xu, G. C. Jose, A. Rutherford, H. Wang, S. Zhang, R. J. Cava, H. Zhou, W. Bi, and W. Xie, Pressure-induced phase transitions in bilayer $\text{La}_3\text{Ni}_2\text{O}_7$, [arXiv:2410.18840](https://arxiv.org/abs/2410.18840) (2024).
 - [24] Y. Li, Y. Cao, L. Liu, P. Peng, H. Lin, C. Pei, M. Zhang, H. Wu, X. Du, W. Zhao, K. Zhai, X. Zhang, J. Zhao, M. Lin, P. Tan, Y. Qi, G. Li, H. Guo, L. Yang, and L. Yang, Distinct ultrafast dynamics

- of bilayer and trilayer nickelate superconductors regarding the density-wave-like transitions, *Sci. Bull.* <https://doi.org/10.1016/j.scib.2024.10.011> (2024).
- [25] Z. Liu, M. Huo, J. Li, Q. Li, Y. Liu, Y. Dai, X. Zhou, J. Hao, Y. Lu, M. Wang, and H.-H. Wen, Electronic correlations and partial gap in the bilayer nickelate $\text{La}_3\text{Ni}_2\text{O}_7$, *Nat. Commun.* **15**, 7570 (2024).
- [26] M. Yashima, N. Seto, Y. Oshita, M. Kakoi, H. Sakurai, Y. Takano, and H. Mukuda, Microscopic evidence for spin–spinless stripe order with reduced Ni moments within *ab* plane for bilayer nickelate $\text{La}_3\text{Ni}_2\text{O}_7$ probed by ^{139}La -NQR, *Journal of the Physical Society of Japan* **94**, 054704 (2025).
- [27] R. Khasanov, V. Sazgari, I. Plokhikh, M. Medarde, E. Pomjakushina, T. Klimczuk, S. Królak, M. J. Winiarski, T. J. Hicken, H. Luetkens, Z. Guguchia, and D. J. Gawryluk, Oxygen-isotope effect on the density wave transitions in $\text{La}_3\text{Ni}_2\text{O}_7$ and $\text{La}_4\text{Ni}_3\text{O}_{10}$, *arXiv:2504.08290* (2025).
- [28] J. Yang, H. Sun, X. Hu, Y. Xie, T. Miao, H. Luo, H. Chen, B. Liang, W. Zhu, G. Qu, C.-Q. Chen, M. Huo, Y. Huang, S. Zhang, F. Zhang, F. Yang, Z. Wang, Q. Peng, H. Mao, G. Liu, Z. Xu, T. Qian, D.-X. Yao, M. Wang, L. Zhao, and X. J. Zhou, Orbital-dependent electron correlation in double-layer nickelate $\text{La}_3\text{Ni}_2\text{O}_7$, *Nat. Commun.* **15**, 4373 (2024).
- [29] L. Wang, Y. Li, S. Xie, F. Liu, H. Sun, C. Huang, Y. Gao, T. Nakagawa, B. Fu, B. Dong, Z. Cao, R. Yu, S. I. Kawaguchi, H. Kadobayashi, M. Wang, C. Jin, H. Kwang Mao, and H. Liu, Structure responsible for the superconducting state in $\text{La}_3\text{Ni}_2\text{O}_7$ at low temperature and high pressure conditions, *Journal of the American Chemical Society* **146**, 7506 (2024).
- [30] T. Cui, S. Choi, T. Lin, C. Liu, G. Wang, N. Wang, S. Chen, H. Hong, D. Rong, Q. Wang, Q. Jin, J.-O. Wang, L. Gu, C. Ge, C. Wang, J. G. Cheng, Q. Zhang, L. Si, K. Juan Jin, and E.-J. Guo, Strain mediated phase crossover in Ruddlesden Popper nickelates, *Communications Materials* **5**, 32 (2024).
- [31] Y. Li, X. Du, Y. Cao, C. Pei, M. Zhang, W. Zhao, K. Zhai, R. Xu, Z. Liu, Z. Li, J. Zhao, G. Li, Y. Qi, H. Guo, Y. Chen, and L. Yang, Electronic correlation and pseudogap-like behavior of high-temperature superconductor $\text{La}_3\text{Ni}_2\text{O}_7$, *Chin. Phys. Lett.* **41**, 087402 (2024).
- [32] M. Li, Y. Wang, C. Pei, M. Zhang, N. Li, J. Guan, M. Amboage, N.-D. Adama, Q. Kong, Y. Qi, and W. Yang, Distinguishing electronic band structure of single-layer and bilayer Ruddlesden-Popper nickelates probed by in-situ high pressure X-ray absorption near-edge spectroscopy, *arXiv:2410.04230* (2024).
- [33] X. Zhou, W. He, Z. Zhou, K. Ni, M. Huo, D. Hu, Y. Zhu, E. Zhang, Z. Jiang, S. Zhang, S. Su, J. Jiang, Y. Yan, Y. Wang, D. Shen, X. Liu, J. Zhao, M. Wang, M. Liu, Z. Du, and D. Feng, Revealing nanoscale structural phase separation in $\text{La}_3\text{Ni}_2\text{O}_{7-\delta}$ single crystal via scanning near-field optical microscopy, *arXiv:2410.06602* (2024).
- [34] G. Wang, N. Wang, T. Lu, S. Calder, J. Yan, L. Shi, J. Hou, L. Ma, L. Zhang, J. Sun, B. Wang, S. Meng, M. Liu, and J. Cheng, Chemical versus physical pressure effects on the structure transition of bilayer nickelates, *npj Quantum Materials* **10**, 1 (2025).
- [35] X. Chen, J. Zhang, A. S. Thind, S. Sharma, H. LaBollita, G. Peterson, H. Zheng, D. P. Phelan, A. S. Botana, R. F. Klie, and J. F. Mitchell, Polymorphism in the Ruddlesden–Popper nickelate $\text{La}_3\text{Ni}_2\text{O}_7$: Discovery of a hidden phase with distinctive layer stacking, *J. Am. Chem. Soc.* **146**, 3640 (2024).
- [36] Z. Dong, M. Huo, J. Li, J. Li, P. Li, H. Sun, L. Gu, Y. Lu, M. Wang, Y. Wang, and Z. Chen, Visualization of oxygen vacancies and self-doped ligand holes in $\text{La}_3\text{Ni}_2\text{O}_{7-\delta}$, *Nature* **630**, 847 (2024).
- [37] F. Li, N. Guo, Q. Zheng, Y. Shen, S. Wang, Q. Cui, C. Liu, S. Wang, X. Tao, G.-M. Zhang, and J. Zhang, Design and synthesis of three-dimensional hybrid Ruddlesden-Popper nickelate single crystals, *Phys. Rev. Mater.* **8**, 053401 (2024).
- [38] P. Puphal, P. Reiss, N. Enderlein, Y.-M. Wu, G. Khalullin, V. Sundaramurthy, T. Priessnitz, M. Knauff, A. Suthar, L. Richter, M. Isobe, P. A. van Aken, H. Takagi, B. Keimer, Y. E. Suyolcu, B. Wehinger, P. Hansmann, and M. Hepting, Unconventional crystal structure of the high-pressure superconductor $\text{La}_3\text{Ni}_2\text{O}_7$, *Phys. Rev. Lett.* **133**, 146002 (2024).
- [39] Y. Zhu, D. Peng, E. Zhang, B. Pan, X. Chen, L. Chen, H. Ren, F. Liu, Y. Hao, N. Li, Z. Xing, F. Lan, J. Han, J. Wang, D. Jia, H. Wo, Y. Gu, Y. Gu, L. Ji, W. Wang, H. Gou, Y. Shen, T. Ying, X. Chen, W. Yang, H. Cao, C. Zheng, Q. Zeng, J.-g. Guo, and J. Zhao, Superconductivity in pressurized trilayer $\text{La}_4\text{Ni}_3\text{O}_{10-\delta}$ single crystals, *Nature* **631**, 531 (2024).
- [40] M. Zhang, C. Pei, D. Peng, X. Du, W. Hu, Y. Cao, Q. Wang, J. Wu, Y. Li, H. Liu, C. Wen, J. Song, Y. Zhao, C. Li, W. Cao, S. Zhu, Q. Zhang, N. Yu, P. Cheng, L. Zhang, Z. Li, J. Zhao, Y. Chen, C. Jin, H. Guo, C. Wu, F. Yang, Q. Zeng, S. Yan, L. Yang, and Y. Qi, Superconductivity in trilayer nickelate $\text{La}_4\text{Ni}_3\text{O}_{10}$ under pressure, *Phys. Rev. X* **15**, 021005 (2025).
- [41] X. Huang, H. Zhang, J. Li, M. Huo, J. Chen, Z. Qiu, P. Ma, C. Huang, H. Sun, and M. Wang, Signature of superconductivity in pressurized trilayer-nickelate $\text{Pr}_4\text{Ni}_3\text{O}_{10-\delta}$, *Chinese Physics Letters* **41**, 127403 (2024).
- [42] Q. Li, Y.-J. Zhang, Z.-N. Xiang, Y. Zhang, X. Zhu, and H.-H. Wen, Signature of superconductivity in pressurized $\text{La}_4\text{Ni}_3\text{O}_{10}$, *Chin. Phys. Lett.* **41**, 017401 (2024).
- [43] J. Zhang, D. Phelan, A. Botana, Y.-S. Chen, H. Zheng, M. Krogstad, S. G. Wang, Y. Qiu, J. Rodriguez-Rivera, R. Osborn, S. Rosenkranz, M. R. Norman, and J. F. Mitchell, Intertwined density waves in a metallic nickelate, *Nat. Commun.* **11**, 6003 (2020).
- [44] S. Xu, C.-Q. Chen, M. Huo, D. Hu, H. Wang, Q. Wu, R. Li, D. Wu, M. Wang, D.-X. Yao, T. Dong, and N. Wang, Origin of the density wave instability in trilayer nickelate $\text{La}_4\text{Ni}_3\text{O}_{10}$ revealed by optical and ultrafast spectroscopy, *Phys. Rev. B* **111**, 075140 (2025).
- [45] X. Du, Y. Li, Y. Cao, C. Pei, M. Zhang, W. Zhao, K. Zhai, R. Xu, Z. Liu, Z. Li, J. Zhao, G. Li, Y. Chen, Y. Qi, H. Guo, and L. Yang, Correlated electronic structure and density-wave gap in trilayer nickelate $\text{La}_4\text{Ni}_3\text{O}_{10}$, *arXiv:2405.19853* (2024).
- [46] D. Li, K. Lee, B. Y. Wang, M. Osada, S. Crossley, H. R. Lee, Y. Cui, Y. Hikita, and H. Y. Hwang, Superconductivity in an infinite-layer nickelate, *Nature* **572**, 624 (2019).
- [47] K. Lee, B. Y. Wang, M. Osada, B. H. Goodge, T. C. Wang, Y. Lee, S. Harvey, W. J. Kim, Y. Yu, C. Murthy,

- S. Raghu, L. F. Kourkoutis, and H. Y. Hwang, Linear-temperature resistivity for optimally superconducting (Nd, Sr) NiO₂, *Nature* **619**, 288 (2023).
- [48] Y. Nomura and R. Arita, Superconductivity in infinite-layer nickelates, *Rep. Prog. Phys.* **85**, 052501 (2022).
- [49] Q. Gu and H.-H. Wen, Superconductivity in nickel-based 112 systems, *The Innovation* **3** (2022).
- [50] X. Sui, X. Han, H. Jin, X. Chen, L. Qiao, X. Shao, and B. Huang, Electronic properties of the bilayer nickelates R₃Ni₂O₇ with oxygen vacancies ($r = \text{La or Ce}$), *Phys. Rev. B* **109**, 205156 (2024).
- [51] Z. Luo, X. Hu, M. Wang, W. Wú, and D.-X. Yao, Bilayer two-orbital model of La₃Ni₂O₇ under pressure, *Phys. Rev. Lett.* **131**, 126001 (2023).
- [52] Y. Zhang, L.-F. Lin, A. Moreo, and E. Dagotto, Electronic structure, dimer physics, orbital-selective behavior, and magnetic tendencies in the bilayer nickelate superconductor La₃Ni₂O₇ under pressure, *Phys. Rev. B* **108**, L180510 (2023).
- [53] Y. Cao and Y.-f. Yang, Flat bands promoted by Hund's rule coupling in the candidate double-layer high-temperature superconductor La₃Ni₂O₇ under high pressure, *Phys. Rev. B* **109**, L081105 (2024).
- [54] Y. Zhang, L.-F. Lin, A. Moreo, T. A. Maier, and E. Dagotto, Structural phase transition, s_{\pm} -wave pairing, and magnetic stripe order in bilayered superconductor La₃Ni₂O₇ under pressure, *Nat. Commun.* **15**, 2470 (2024).
- [55] J. Huang, Z. D. Wang, and T. Zhou, Impurity and vortex states in the bilayer high-temperature superconductor La₃Ni₂O₇, *Phys. Rev. B* **108**, 174501 (2023).
- [56] B. Geisler, J. J. Hamlin, G. R. Stewart, R. G. Hennig, and P. Hirschfeld, Structural transitions, octahedral rotations, and electronic properties of A₃Ni₂O₇ rare-earth nickelates under high pressure, *npj Quantum Materials* **9**, 38 (2024).
- [57] L. C. Rhodes and P. Wahl, Structural routes to stabilize superconducting La₃Ni₂O₇ at ambient pressure, *Phys. Rev. Mater.* **8**, 044801 (2024).
- [58] Y. Zhang, L.-F. Lin, A. Moreo, T. A. Maier, and E. Dagotto, Electronic structure, magnetic correlations, and superconducting pairing in the reduced Ruddlesden-Popper bilayer La₃Ni₂O₆ under pressure: Different role of $d_{3z^2-r^2}$ orbital compared with La₃Ni₂O₇, *Phys. Rev. B* **109**, 045151 (2024).
- [59] N. Yuan, A. Elghandour, J. Arneht, K. Dey, and R. Klingeler, High-pressure crystal growth and investigation of the metal-to-metal transition of Ruddlesden-Popper trilayer nickelates La₄Ni₃O₁₀, *J. Cryst. Growth* **627**, 127511 (2024).
- [60] J. Li, C.-Q. Chen, C. Huang, Y. Han, M. Huo, X. Huang, P. Ma, Z. Qiu, J. Chen, X. Hu, L. Chen, T. Xie, B. Shen, H. Sun, D. Yao, and M. Wang, Structural transition, electric transport, and electronic structures in the compressed trilayer nickelate La₄Ni₃O₁₀, *Sci. China Phys. Mech. Astron.* **67**, 117403 (2024).
- [61] B. Geisler, L. Fanfarillo, J. J. Hamlin, G. R. Stewart, R. G. Hennig, and P. J. Hirschfeld, Optical properties and electronic correlations in La₃Ni₂O_{7- δ} bilayer nickelates under high pressure, *npj Quantum Materials* **9**, 89 (2024).
- [62] H. Li, X. Zhou, T. Nummy, J. Zhang, V. Pardo, W. E. Pickett, J. F. Mitchell, and D. S. Dessau, Fermiology and electron dynamics of trilayer nickelate La₄Ni₃O₁₀, *Nat. Commun.* **8**, 704 (2017).
- [63] J.-X. Wang, Z. Ouyang, R.-Q. He, and Z.-Y. Lu, Non-Fermi liquid and Hund correlation in La₄Ni₃O₁₀ under high pressure, *Phys. Rev. B* **109**, 165140 (2024).
- [64] C.-Q. Chen, Z. Luo, M. Wang, W. Wú, and D.-X. Yao, Trilayer multiorbital models of La₄Ni₃O₁₀, *Phys. Rev. B* **110**, 014503 (2024).
- [65] Y. Shen, M. Qin, and G.-M. Zhang, Effective bilayer model hamiltonian and density-matrix renormalization group study for the high- T_c superconductivity La₃Ni₂O₇ under high pressure, *Chin. Phys. Lett.* **40**, 127401 (2023).
- [66] V. Christiansson, F. Petocchi, and P. Werner, Correlated electronic structure of La₃Ni₂O₇ under pressure, *Phys. Rev. Lett.* **131**, 206501 (2023).
- [67] D. A. Shilenko and I. V. Leonov, Correlated electronic structure, orbital-selective behavior, and magnetic correlations in double-layer La₃Ni₂O₇ under pressure, *Phys. Rev. B* **108**, 125105 (2023).
- [68] W. Wú, Z. Luo, D.-X. Yao, and M. Wang, Superexchange and charge transfer in the nickelate superconductor La₃Ni₂O₇ under pressure, *Sci. China-Phys. Mech. Astron.* **67**, 117402 (2024).
- [69] X. Chen, P. Jiang, J. Li, Z. Zhong, and Y. Lu, Charge and spin instabilities in superconducting La₃Ni₂O₇, *Phys. Rev. B* **111**, 014515 (2025).
- [70] Z. Ouyang, J.-M. Wang, J.-X. Wang, R.-Q. He, L. Huang, and Z.-Y. Lu, Hund electronic correlation in La₃Ni₂O₇ under high pressure, *Phys. Rev. B* **109**, 115114 (2024).
- [71] G. Heier, K. Park, and S. Y. Savrasov, Competing d_{xy} and s_{\pm} pairing symmetries in superconducting La₃Ni₂O₇: LDA + FLEX calculations, *Phys. Rev. B* **109**, 104508 (2024).
- [72] Y. Wang, K. Jiang, Z. Wang, F.-C. Zhang, and J. Hu, Electronic and magnetic structures of bilayer la₃ni₂o₇ at ambient pressure, *Phys. Rev. B* **110**, 205122 (2024).
- [73] S. Bötzel, F. Lechermann, J. Gondolf, and I. M. Eremin, Theory of magnetic excitations in multilayer nickelate superconductor La₃Ni₂O₇, *Phys. Rev. B* **109**, L180502 (2024).
- [74] Q.-G. Yang, D. Wang, and Q.-H. Wang, Possible S_{\pm} -wave superconductivity in La₃Ni₂O₇, *Phys. Rev. B* **108**, L140505 (2023).
- [75] Y.-B. Liu, J.-W. Mei, F. Ye, W.-Q. Chen, and F. Yang, s^{\pm} -wave pairing and the destructive role of apical-oxygen deficiencies in La₃Ni₂O₇ under pressure, *Phys. Rev. Lett.* **131**, 236002 (2023).
- [76] F. Lechermann, J. Gondolf, S. Bötzel, and I. M. Eremin, Electronic correlations and superconducting instability in La₃Ni₂O₇ under high pressure, *Phys. Rev. B* **108**, L201121 (2023).
- [77] H. Sakakibara, N. Kitamine, M. Ochi, and K. Kuroki, Possible high T_c superconductivity in La₃Ni₂O₇ under high pressure through manifestation of a nearly half-filled bilayer Hubbard model, *Phys. Rev. Lett.* **132**, 106002 (2024).
- [78] Y. Gu, C. Le, Z. Yang, X. Wu, and J. Hu, Effective model and pairing tendency in the bilayer Ni-based superconductor La₃Ni₂O₇, *Phys. Rev. B* **111**, 174506 (2025).
- [79] C. Lu, Z. Pan, F. Yang, and C. Wu, Interlayer-coupling-driven high-temperature superconductivity in La₃Ni₂O₇ under pressure, *Phys. Rev. Lett.* **132**, 146002 (2024).

- [80] H. Oh and Y.-H. Zhang, Type-II t - J model and shared superexchange coupling from Hund's rule in superconducting $\text{La}_3\text{Ni}_2\text{O}_7$, *Phys. Rev. B* **108**, 174511 (2023).
- [81] Z. Liao, L. Chen, G. Duan, Y. Wang, C. Liu, R. Yu, and Q. Si, Electron correlations and superconductivity in $\text{La}_3\text{Ni}_2\text{O}_7$ under pressure tuning, *Phys. Rev. B* **108**, 214522 (2023).
- [82] X.-Z. Qu, D.-W. Qu, J. Chen, C. Wu, F. Yang, W. Li, and G. Su, Bilayer t - J - J_\perp model and magnetically mediated pairing in the pressurized nickelate $\text{La}_3\text{Ni}_2\text{O}_7$, *Phys. Rev. Lett.* **132**, 036502 (2024).
- [83] Y.-F. Yang, G.-M. Zhang, and F.-C. Zhang, Interlayer valence bonds and two-component theory for high- T_c superconductivity of $\text{La}_3\text{Ni}_2\text{O}_7$ under pressure, *Phys. Rev. B* **108**, L201108 (2023).
- [84] K. Jiang, Z. Wang, and F.-C. Zhang, High temperature superconductivity in $\text{La}_3\text{Ni}_2\text{O}_7$, *Chin. Phys. Lett.* (2023).
- [85] Y. Zhang, L.-F. Lin, A. Moreo, T. A. Maier, and E. Dagotto, Trends in electronic structures and s_{\pm} -wave pairing for the rare-earth series in bilayer nickelate superconductor $R_3\text{Ni}_2\text{O}_7$, *Phys. Rev. B* **108**, 165141 (2023).
- [86] Q. Qin and Y.-F. Yang, High- T_c superconductivity by mobilizing local spin singlets and possible route to higher T_c in pressurized $\text{La}_3\text{Ni}_2\text{O}_7$, *Phys. Rev. B* **108**, L140504 (2023).
- [87] Y.-H. Tian, Y. Chen, J.-M. Wang, R.-Q. He, and Z.-Y. Lu, Correlation effects and concomitant two-orbital s_{\pm} -wave superconductivity in $\text{La}_3\text{Ni}_2\text{O}_7$ under high pressure, *Phys. Rev. B* **109**, 165154 (2024).
- [88] R. Jiang, J. Hou, Z. Fan, Z.-J. Lang, and W. Ku, Pressure driven fractionalization of ionic spins results in cupratelike high- T_c superconductivity in $\text{La}_3\text{Ni}_2\text{O}_7$, *Phys. Rev. Lett.* **132**, 126503 (2024).
- [89] D.-C. Lu, M. Li, Z.-Y. Zeng, W. Hou, J. Wang, F. Yang, and Y.-Z. You, Superconductivity from doping symmetric mass generation insulators: Application to $\text{La}_3\text{Ni}_2\text{O}_7$ under pressure, [arXiv:2308.11195](https://arxiv.org/abs/2308.11195) (2023).
- [90] N. Kitamine, M. Ochi, and K. Kuroki, Theoretical designing of multiband nickelate and palladate superconductors with $d^{8+\delta}$ configuration, [arXiv:2308.12750](https://arxiv.org/abs/2308.12750) (2023).
- [91] Z. Luo, B. Lv, M. Wang, W. Wú, and D.-X. Yao, High- T_c superconductivity in $\text{La}_3\text{Ni}_2\text{O}_7$ based on the bilayer two-orbital t - J model, *npj Quantum Materials* **9**, 61 (2024).
- [92] J.-X. Zhang, H.-K. Zhang, Y.-Z. You, and Z.-Y. Weng, Strong pairing originated from an emergent \mathbb{Z}_2 berry phase in $\text{La}_3\text{Ni}_2\text{O}_7$, *Phys. Rev. Lett.* **133**, 126501 (2024).
- [93] Z. Pan, C. Lu, F. Yang, and C. Wu, Effect of rare-earth element substitution in superconducting $R_3\text{Ni}_2\text{O}_7$ under pressure, *Chinese Physics Letters* **41**, 087401 (2024).
- [94] H. Sakakibara, M. Ochi, H. Nagata, Y. Ueki, H. Sakurai, R. Matsumoto, K. Terashima, K. Hirose, H. Ohta, M. Kato, Y. Takano, and K. Kuroki, Theoretical analysis on the possibility of superconductivity in the trilayer Ruddlesden-Popper nickelate $\text{La}_4\text{Ni}_3\text{O}_{10}$ under pressure and its experimental examination: Comparison with $\text{La}_3\text{Ni}_2\text{O}_7$, *Phys. Rev. B* **109**, 144511 (2024).
- [95] H. Lange, L. Homeier, E. Demler, U. Schollwöck, A. Bohrdt, and F. Grusdt, Pairing dome from an emergent Feshbach resonance in a strongly repulsive bilayer model, *Phys. Rev. B* **110**, L081113 (2024).
- [96] H. Yang, H. Oh, and Y.-H. Zhang, Strong pairing from a small Fermi surface beyond weak coupling: Application to $\text{La}_3\text{Ni}_2\text{O}_7$, *Phys. Rev. B* **110**, 104517 (2024).
- [97] H. Lange, L. Homeier, E. Demler, U. Schollwöck, F. Grusdt, and A. Bohrdt, Feshbach resonance in a strongly repulsive ladder of mixed dimensionality: A possible scenario for bilayer nickelate superconductors, *Phys. Rev. B* **109**, 045127 (2024).
- [98] T. Kaneko, H. Sakakibara, M. Ochi, and K. Kuroki, Pair correlations in the two-orbital Hubbard ladder: Implications for superconductivity in the bilayer nickelate $\text{La}_3\text{Ni}_2\text{O}_7$, *Phys. Rev. B* **109**, 045154 (2024).
- [99] Z. Fan, J.-F. Zhang, B. Zhan, D. Lv, X.-Y. Jiang, B. Normand, and T. Xiang, Superconductivity in nickelate and cuprate superconductors with strong bilayer coupling, *Phys. Rev. B* **110**, 024514 (2024).
- [100] X. Wu, H. Yang, and Y.-H. Zhang, Deconfined Fermi liquid to Fermi liquid transition and superconducting instability, *Phys. Rev. B* **110**, 125122 (2024).
- [101] Y. Zhang, L.-F. Lin, A. Moreo, T. A. Maier, and E. Dagotto, Prediction of s^{\pm} -wave superconductivity enhanced by electronic doping in trilayer nickelates $\text{La}_4\text{Ni}_3\text{O}_{10}$ under pressure, *Phys. Rev. Lett.* **133**, 136001 (2024).
- [102] M. Zhang, H. Sun, Y.-B. Liu, Q. Liu, W.-Q. Chen, and F. Yang, The s^{\pm} -wave superconductivity in the pressurized $\text{La}_4\text{Ni}_3\text{O}_{10}$, *Phys. Rev. B* **110**, L180501 (2024).
- [103] Q.-G. Yang, K.-Y. Jiang, D. Wang, H.-Y. Lu, and Q.-H. Wang, Effective model and s_{\pm} -wave superconductivity in trilayer nickelate $\text{La}_4\text{Ni}_3\text{O}_{10}$, *Phys. Rev. B* **109**, L220506 (2024).
- [104] Y. Zhang, L.-F. Lin, A. Moreo, T. A. Maier, and E. Dagotto, Electronic structure, self-doping, and superconducting instability in the alternating single-layer trilayer stacking nickelates $\text{La}_3\text{Ni}_2\text{O}_7$, *Phys. Rev. B* **110**, L060510 (2024).
- [105] Y.-F. Yang, Decomposition of multilayer superconductivity with interlayer pairing, *Phys. Rev. B* **110**, 104507 (2024).
- [106] S. Ryee, N. Witt, and T. O. Wehling, Quenched pair breaking by interlayer correlations as a key to superconductivity in $\text{La}_3\text{Ni}_2\text{O}_7$, *Phys. Rev. Lett.* **133**, 096002 (2024).
- [107] C. Lu, Z. Pan, F. Yang, and C. Wu, Interplay of two E_g orbitals in superconducting $\text{La}_3\text{Ni}_2\text{O}_7$ under pressure, *Phys. Rev. B* **110**, 094509 (2024).
- [108] Z. Ouyang, M. Gao, and Z.-Y. Lu, Absence of electron-phonon coupling superconductivity in the bilayer phase of $\text{La}_3\text{Ni}_2\text{O}_7$ under pressure, *npj Quantum Materials* **9**, 80 (2024).
- [109] H. LaBollita, V. Pardo, M. R. Norman, and A. S. Botana, Electronic structure and magnetic properties of $\text{La}_3\text{Ni}_2\text{O}_7$ under pressure: active role of the $\text{Ni-}d_{x^2-y^2}$ orbitals, [arXiv:2309.17279](https://arxiv.org/abs/2309.17279) (2024).
- [110] B. Zhang, C. Xu, and H. Xiang, Emergent spin-charge-orbital order in superconductor $\text{La}_3\text{Ni}_2\text{O}_7$, [arXiv:2407.18473](https://arxiv.org/abs/2407.18473) (2024).
- [111] I. V. Leonov, Electronic correlations and spin-charge-density stripes in double-layer $\text{La}_3\text{Ni}_2\text{O}_7$, [arXiv:2410.15298](https://arxiv.org/abs/2410.15298) (2024).
- [112] H. LaBollita, V. Pardo, M. R. Norman, and A. S. Botana, Assessing spin-density wave formation in $\text{La}_3\text{Ni}_2\text{O}_7$ from electronic structure calculations, *Phys.*

- Rev. Mater.* **8**, L111801 (2024).
- [113] X.-S. Ni, Y. Ji, L. He, T. Xie, D.-X. Yao, M. Wang, and K. Cao, Spin density wave in the bilayered nickelate $\text{La}_3\text{Ni}_2\text{O}_{7-\delta}$ at ambient pressure, *npj Quantum Materials* **10**, 17 (2025).
- [114] X.-W. Yi, Y. Meng, J.-W. Li, Z.-W. Liao, W. Li, J.-Y. You, B. Gu, and G. Su, Nature of charge density waves and metal-insulator transition in pressurized $\text{La}_3\text{Ni}_2\text{O}_7$, *Phys. Rev. B* **110**, L140508 (2024).
- [115] H. LaBollita, J. Kapeghian, M. R. Norman, and A. S. Botana, Electronic structure and magnetic tendencies of trilayer $\text{La}_4\text{Ni}_3\text{O}_{10}$ under pressure: Structural transition, molecular orbitals, and layer differentiation, *Phys. Rev. B* **109**, 195151 (2024).
- [116] K.-Y. Jiang, Y.-H. Cao, Q.-G. Yang, H.-Y. Lu, and Q.-H. Wang, Theory of pressure dependence of superconductivity in bilayer nickelate $\text{La}_3\text{Ni}_2\text{O}_7$, *Phys. Rev. Lett.* **134**, 076001 (2025).
- [117] Y. Chen, Y.-H. Tian, J.-M. Wang, R.-Q. He, and Z.-Y. Lu, Non-Fermi liquid and antiferromagnetic correlations with hole doping in the bilayer two-orbital Hubbard model of $\text{La}_3\text{Ni}_2\text{O}_7$ at zero temperature, *Phys. Rev. B* **110**, 235119 (2024).
- [118] Y. Zhang, L.-F. Lin, A. Moreo, T. A. Maier, and E. Dagotto, Magnetic correlations and pairing tendencies of the hybrid stacking nickelate superlattice $\text{La}_7\text{Ni}_5\text{O}_{17}$ ($\text{La}_3\text{Ni}_2\text{O}_7/\text{La}_4\text{Ni}_3\text{O}_{10}$) under pressure, *arXiv:2408.07690* (2024).
- [119] L.-F. Lin, Y. Zhang, N. Kaushal, G. Alvarez, T. A. Maier, A. Moreo, and E. Dagotto, Magnetic phase diagram of a two-orbital model for bilayer nickelates with varying doping, *Phys. Rev. B* **110**, 195135 (2024).
- [120] G. Jiang, C. Qin, K. Foyevtsova, L. Si, M. Berciu, G. A. Sawatzky, and M. Jiang, Intertwined charge and spin instability of $\text{La}_3\text{Ni}_2\text{O}_7$, *arXiv:2410.15649* (2024).
- [121] I. V. Leonov, Electronic structure and magnetic correlations in the trilayer nickelate superconductor $\text{La}_4\text{Ni}_3\text{O}_{10}$ under pressure, *Phys. Rev. B* **109**, 235123 (2024).
- [122] Y. Liu, M. Ou, H. Chu, H. Yang, Q. Li, Y.-J. Zhang, and H.-H. Wen, Growth and characterization of the $\text{La}_3\text{Ni}_2\text{O}_{7-\delta}$ thin films: Dominant contribution of the $d_{x^2-y^2}$ orbital at ambient pressure, *Phys. Rev. Mater.* **8**, 124801 (2024).
- [123] Y. Liu, M. Ou, Y. Wang, and H.-H. Wen, Decoupling between $d_{x^2-y^2}$ and d_{z^2} orbitals in hole doped $\text{La}_3\text{Ni}_2\text{O}_7$, *arXiv:2411.16047* (2024).
- [124] Y. Tian and Y. Chen, Spin density wave and superconductivity in the bilayer t - J model of $\text{La}_3\text{Ni}_2\text{O}_7$ under renormalized mean-field theory, *arXiv:2412.17453* (2024).
- [125] Y. Yin, J. Zhan, B. Liu, and X. Han, The s_{\pm} pairing symmetry in the pressured $\text{La}_3\text{Ni}_2\text{O}_7$ from electron-phonon coupling, *arXiv:2502.21016* (2025).
- [126] W. Xi, S.-L. Yu, and J.-X. Li, Transition from s_{\pm} -wave to $d_{x^2-y^2}$ -wave superconductivity driven by interlayer interaction in the bilayer two-orbital model of $\text{La}_3\text{Ni}_2\text{O}_7$, *Phys. Rev. B* **111**, 104505 (2025).
- [127] T. Kaneko, M. Kakoi, and K. Kuroki, t - J model for strongly correlated two-orbital systems: Application to bilayer nickelate superconductors, *arxiv:2504.10114* (2025).
- [128] J.-H. Ji, C. Lu, Z.-Y. Shao, Z. Pan, F. Yang, and C. Wu, A strong-coupling-limit study on the pairing mechanism in the pressurized $\text{La}_3\text{Ni}_2\text{O}_7$, *arxiv:2504.12127* (2025).
- [129] Y. Wang, Y. Zhang, and K. Jiang, Electronic structure and disorder effect of $\text{La}_3\text{Ni}_2\text{O}_7$ superconductor, *Chinese Physics B* **34**, 047105 (2025).
- [130] M. E. Haque, R. Ali, M. Masum, J. Hassan, and S. Naqib, DFT exploration of pressure dependent physical properties of the recently discovered $\text{La}_3\text{Ni}_2\text{O}_7$ superconductor, *arXiv:2504.15853* (2025).
- [131] L. Shi, Y. Luo, W. Wu, and Y. Zhang, Theoretical investigation of high- T_c superconductivity in Sr-doped $\text{La}_3\text{Ni}_2\text{O}_7$ at ambient pressure, *arXiv:2503.13197* (2025).
- [132] E. K. Ko, Y. Yu, Y. Liu, L. Bhatt, J. Li, V. Thampy, C.-T. Kuo, B. Y. Wang, Y. Lee, K. Lee, J.-S. Lee, B. H. Goodge, D. A. Muller, and H. Y. Hwang, Signatures of ambient pressure superconductivity in thin film $\text{La}_3\text{Ni}_2\text{O}_7$, *Nature* **638**, 935 (2025).
- [133] G. Zhou, W. Lv, H. Wang, Z. Nie, Y. Chen, Y. Li, H. Huang, W. Chen, Y. Sun, Q.-K. Xue, *et al.*, Ambient-pressure superconductivity onset above 40 K in $(\text{La}, \text{Pr})_3\text{Ni}_2\text{O}_7$ films, *Nature* **640**, 641 (2025).
- [134] Y. Liu, E. K. Ko, Y. Tarn, L. Bhatt, B. H. Goodge, D. A. Muller, S. Raghu, Y. Yu, and H. Y. Hwang, Superconductivity and normal-state transport in compressively strained $\text{La}_2\text{PrNi}_2\text{O}_7$ thin films, *arXiv:2501.08022* (2025).
- [135] C. Yue, J.-J. Miao, H. Huang, Y. Hua, P. Li, Y. Li, G. Zhou, W. Lv, Q. Yang, H. Sun, Y.-J. Sun, J. Lin, Q.-K. Xue, Z. Chen, and W.-Q. Chen, Correlated electronic structures and unconventional superconductivity in bilayer nickelate heterostructures, *arXiv:2501.06875* (2025).
- [136] P. Li, G. Zhou, W. Lv, Y. Li, C. Yue, H. Huang, L. Xu, J. Shen, Y. Miao, W. Song, z. Nie, Y. Chen, H. Wang, W. Chen, Y. Huang, Z.-H. Chen, T. Qian, J. Lin, J. He, Y.-J. Sun, Z. Chen, and Q.-K. Xue, Photoemission evidence for multi-orbital hole-doping in superconducting $\text{La}_{2.85}\text{Pr}_{0.15}\text{Ni}_2\text{O}_7/\text{SrLaAlO}_4$ interfaces, *arXiv:2501.09255* (2025).
- [137] L. Bhatt, A. Y. Jiang, E. K. Ko, N. Schnitzer, G. A. Pan, D. F. Segedin, Y. Liu, Y. Yu, Y.-F. Zhao, E. A. Morales, C. M. Brooks, A. S. Botana, H. Y. Hwang, J. A. Mundy, D. A. Muller, and B. H. Goodge, Resolving structural origins for superconductivity in strain-engineered $\text{La}_3\text{Ni}_2\text{O}_7$ thin films, *arXiv:2501.08204* (2025).
- [138] Z.-Y. Shao, Y.-B. Liu, M. Liu, and F. Yang, Band structure and pairing nature of $\text{La}_3\text{Ni}_2\text{O}_7$ thin film at ambient pressure, *arXiv:2501.10409* (2025).
- [139] H. Shi, Z. Huo, G. Li, H. Ma, T. Cui, D.-X. Yao, and D. Duan, The effect of carrier doping and thickness on the electronic structures of $\text{La}_3\text{Ni}_2\text{O}_7$ thin films, *arXiv:2502.04255* (2025).
- [140] C. Le, J. Zhan, X. Wu, and J. Hu, Landscape of correlated orders in strained bilayer nickelate thin films, *arXiv:2501.14665* (2025).
- [141] X. Hu, W. Qiu, C.-Q. Chen, Z. Luo, and D.-X. Yao, Electronic structures and multi-orbital models of $\text{La}_3\text{Ni}_2\text{O}_7$ thin films at ambient pressure, *arXiv:2503.17223* (2025).
- [142] B. Y. Wang, Y. Zhong, S. Abadi, Y. Liu, Y. Yu, X. Zhang, Y.-M. Wu, R. Wang, J. Li, Y. Tarn, E. K. Ko, V. Thampy, M. Hashimoto, D. Lu, Y. S. Lee, T. P. Devereaux, C. Jia, H. Y. Hwang, and Z.-X. Shen, Electronic structure of compressively strained thin film

- $\text{La}_2\text{PrNi}_2\text{O}_7$, [arxiv:2504.16372 \(2025\)](#).
- [143] J. Huang and T. Zhou, s_{\pm} pairing via interlayer interaction in $\text{La}_{2.85}\text{Pr}_{0.15}\text{Ni}_2\text{O}_7$ thin films under ambient pressure, [arXiv:2503.23861 \(2025\)](#).
- [144] B. Geisler, J. J. Hamlin, G. R. Stewart, R. G. Hennig, and P. Hirschfeld, Electronic reconstruction and interface engineering of emergent spin fluctuations in compressively strained $\text{La}_3\text{Ni}_2\text{O}_7$ on $\text{SrLaAlO}_4(001)$, [arXiv:2503.10902 \(2025\)](#).
- [145] P. J. Phillips, X. Rui, A. B. Georgescu, A. S. Disa, P. Longo, E. Okunishi, F. Walker, C. H. Ahn, S. Ismail-Beigi, and R. F. Klie, Experimental verification of orbital engineering at the atomic scale: Charge transfer and symmetry breaking in nickelate heterostructures, *Phys. Rev. B* **95**, 205131 (2017).
- [146] S. Lee, A. T. Lee, A. B. Georgescu, G. Fabbris, M.-G. Han, Y. Zhu, J. W. Freeland, A. S. Disa, Y. Jia, M. P. M. Dean, F. J. Walker, S. Ismail-Beigi, and C. H. Ahn, Strong orbital polarization in a cobaltate-titanate oxide heterostructure, *Phys. Rev. Lett.* **123**, 117201 (2019).
- [147] R. U. Chandrasena, C. L. Flint, W. Yang, A. Arab, S. Nemšák, M. Gehlmann, V. B. Özdöl, F. Bisti, K. D. Wijesekara, J. Meyer-Ilse, E. Gullikson, E. Arenholz, J. Ciston, C. M. Schneider, V. N. Strocov, Y. Suzuki, and A. X. Gray, Depth-resolved charge reconstruction at the $\text{LaNiO}_3/\text{CaMnO}_3$ interface, *Phys. Rev. B* **98**, 155103 (2018).
- [148] J. R. Paudel, M. Terilli, T.-C. Wu, J. D. Grassi, A. M. Derrico, R. K. Sah, M. Kareev, F. Wen, C. Klewe, P. Shafer, A. Gloskovskii, C. Schlueter, V. N. Strocov, J. Chakhalian, and A. X. Gray, Direct experimental evidence of tunable charge transfer at the $\text{LaNiO}_3/\text{CaMnO}_3$ ferromagnetic interface, *Phys. Rev. B* **108**, 054441 (2023).
- [149] D. Mondal, S. R. Mahapatra, A. M. Derrico, R. K. Rai, J. R. Paudel, C. Schlueter, A. Gloskovskii, R. Banerjee, A. Hariki, F. M. DeGroot, *et al.*, Modulation-doping a correlated electron insulator, *Nature Communications* **14**, 6210 (2023).
- [150] J. R. Paudel, A. M. Tehrani, M. Terilli, M. Kareev, J. Grassi, R. K. Sah, L. Wu, V. N. Strocov, C. Klewe, P. Shafer, J. Chakhalian, N. A. Spaldin, and A. X. Gray, Depth-resolved profile of the interfacial ferromagnetism in $\text{CaMnO}_3/\text{CaRuO}_3$ superlattices, *Nano Letters* **24**, 15195 (2024).
- [151] J. Jiang, A. T. Lee, S. Lee, C. Lau, M. Li, T. M. Pedersen, C. Liu, S. Gorovikov, S. Zhdanovich, A. Damascelli, K. Zou, F. J. Walker, S. Ismail-Beigi, and C. H. Ahn, Electronic properties of epitaxial $\text{La}_{1-x}\text{Sr}_x\text{RhO}_3$ thin films, *Phys. Rev. B* **103**, 195153 (2021).
- [152] B. Sohn, G. Marcaud, Y. Shin, S. Lee, T. Werner, T. Yilmaz, J. Yang, W. Wei, A. Fedorov, E. Vescovo, Y. He, S. Ismail-Beigi, C. H. Ahn, and F. J. Walker, Observation of orbital selective charge transfer in a Fe/BaTiO_3 interfacial two-dimensional electron gas, *Phys. Rev. B* **109**, 155106 (2024).
- [153] Y. Cao, D. Rodan-Legrain, O. Rubies-Bigorda, J. M. Park, K. Watanabe, T. Taniguchi, and P. Jarillo-Herrero, Tunable correlated states and spin-polarized phases in twisted bilayer–bilayer graphene, *Nature* **583**, 215 (2020).
- [154] H. Zhang, Q. Li, Y. Park, Y. Jia, W. Chen, J. Li, Q. Liu, C. Bao, N. Leconte, S. Zhou, Y. Wang, K. Watanabe, T. Taniguchi, J. Avila, P. Dudin, P. Yu, H. Weng, W. Duan, Q. Wu, J. Jung, and S. Zhou, Observation of dichotomic field-tunable electronic structure in twisted monolayer-bilayer graphene, *Nature Communications* **15**, 3737 (2024).
- [155] Z. Zhou, J. Jiang, P. Karnatak, Z. Wang, G. Wagner, K. Watanabe, T. Taniguchi, C. Schönenberger, S. Parameswaran, S. H. Simon, and M. Banerjee, Gate-tunable double-dome superconductivity in twisted trilayer graphene, *Nature Physics* (2025).
- [156] G. Kotliar and J. Liu, Superexchange mechanism and d -wave superconductivity, *Phys. Rev. B* **38**, 5142 (1988).
- [157] See Supplementary Information at [URL], in which Sec. A and B provide details of the SBMF method for the single-orbital and two-orbital models, respectively, along with additional figures, Sec. C shows more results of the DMRG study for the single-orbital model, and Sec. D shows the effect of the interlayer Coulomb interaction.
- [158] S. R. White, Density-matrix algorithms for quantum renormalization groups, *Phys. Rev. B* **48**, 10345 (1993).
- [159] Y. L. Lee, Y. W. Lee, C.-Y. Mou, and Z. Y. Weng, Two-leg $t - J$ ladder: A mean-field description, *Phys. Rev. B* **60**, 13418 (1999).
- [160] Jutho, L. Devos, M. Hauru, maartenvd, ho oto, Gertian, L. Burgelman, tangwei94, J. TagBot, S. Carlström, V. Vanthilt, Xiaoyu, and qmortier, [Jutho/tensorkit.jl:v0.12.7 \(2024\)](#).
- [161] Q. Li, [FiniteMPS.jl \(2025\)](#).
- [162] A. Weichselbaum, Non-abelian symmetries in tensor networks: A quantum symmetry space approach, *Annals of Physics* **327**, 2972 (2012).
- [163] A. Weichselbaum, X-symbols for non-abelian symmetries in tensor networks, *Phys. Rev. Res.* **2**, 023385 (2020).